Electronic Supplementary Material (ESI) for Dalton Transactions.

Mononuclear ruthenium compounds bearing N-donor and N-heterocyclic carbene ligands: structure and oxidative catalysis

H.-J. Liu,[a] M. Gil-Sepulcre,[a] L. Francàs,[b] P. Nolis,[c] T. Parella,[c] J. Benet-Buchholz,[b] X. Fontrodona,[d] J. García-Antón,[a] N. Romero,[a] A. Llobet,[a,b] L. Escriche,*[a] R. Bofill*[a] and X. Sala*[a]

---

[a] Departament de Química, Facultat de Ciències, Universitat Autònoma de Barcelona, Cerdanyola del Vallès, 08193 Barcelona (Catalonia), Spain. E-mail: roger.bofill@uab.cat, lluis.escriche@uab.cat, xavier.sala@uab.cat. Fax: + 34 93 581 24 77

[b] Institute of Chemical Research of Catalonia (ICIQ), Av. Països Catalans 16, 43007 Tarragona (Catalonia), Spain.

[c] Servei de Ressonància Magnètica Nuclear, Facultat de Ciències, Universitat Autònoma de Barcelona, Cerdanyola del Vallès, 08193 Barcelona (Catalonia), Spain.

[d] Serveis Tècnics de Recerca, Edifici P-II, Campus Montilivi, Universitat de Girona, 17071 Girona (Catalonia), Spain.

Figure S1. 1D and 2D NMR spectra of ligand H_2**L1**$(PF_6)_2$ (600 MHz, 298K, acetone-d_6): a) 1D $^{13}C\{^1H\}$, b) 2D HSQC, c) 2D HMBC.

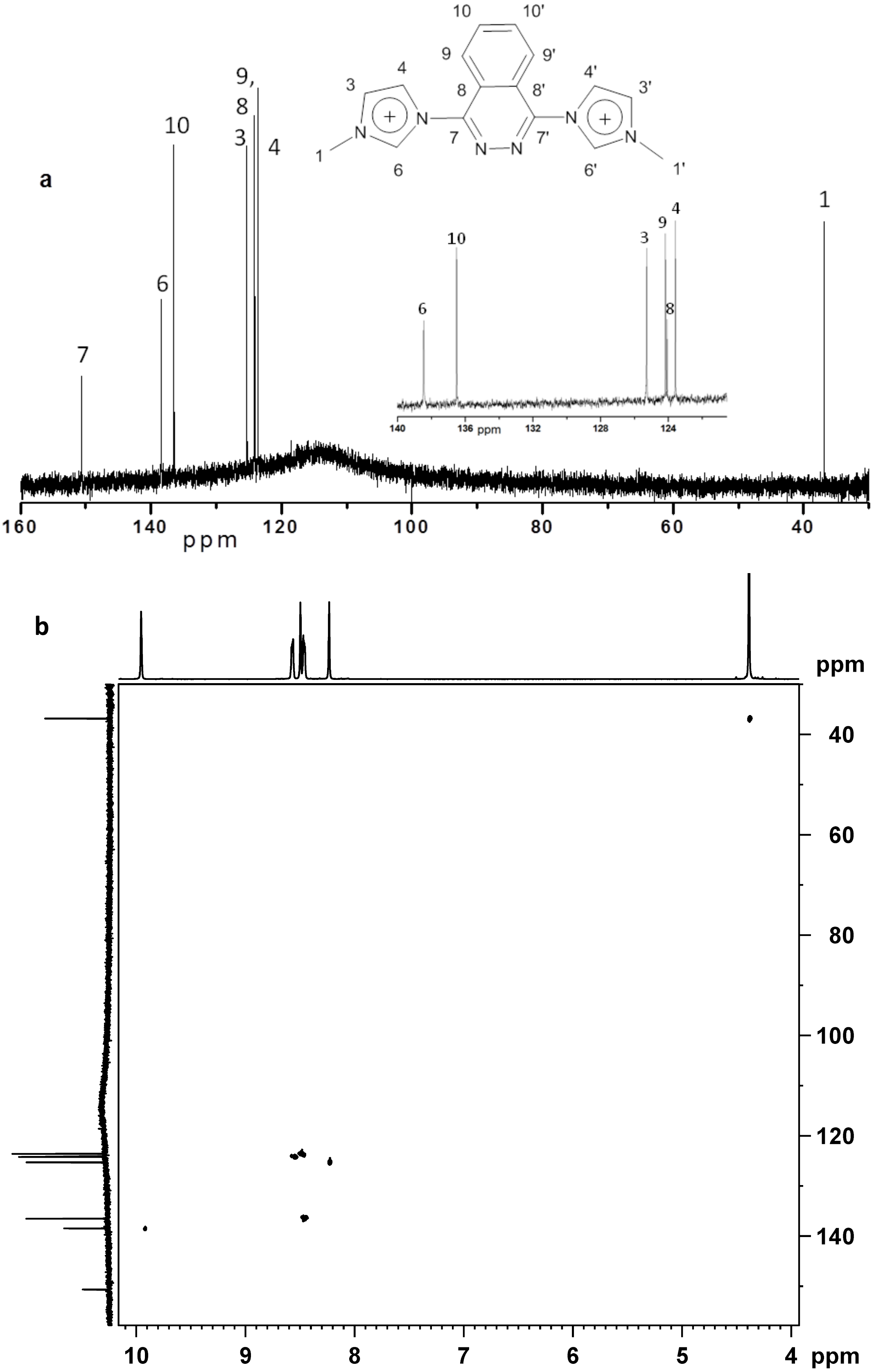

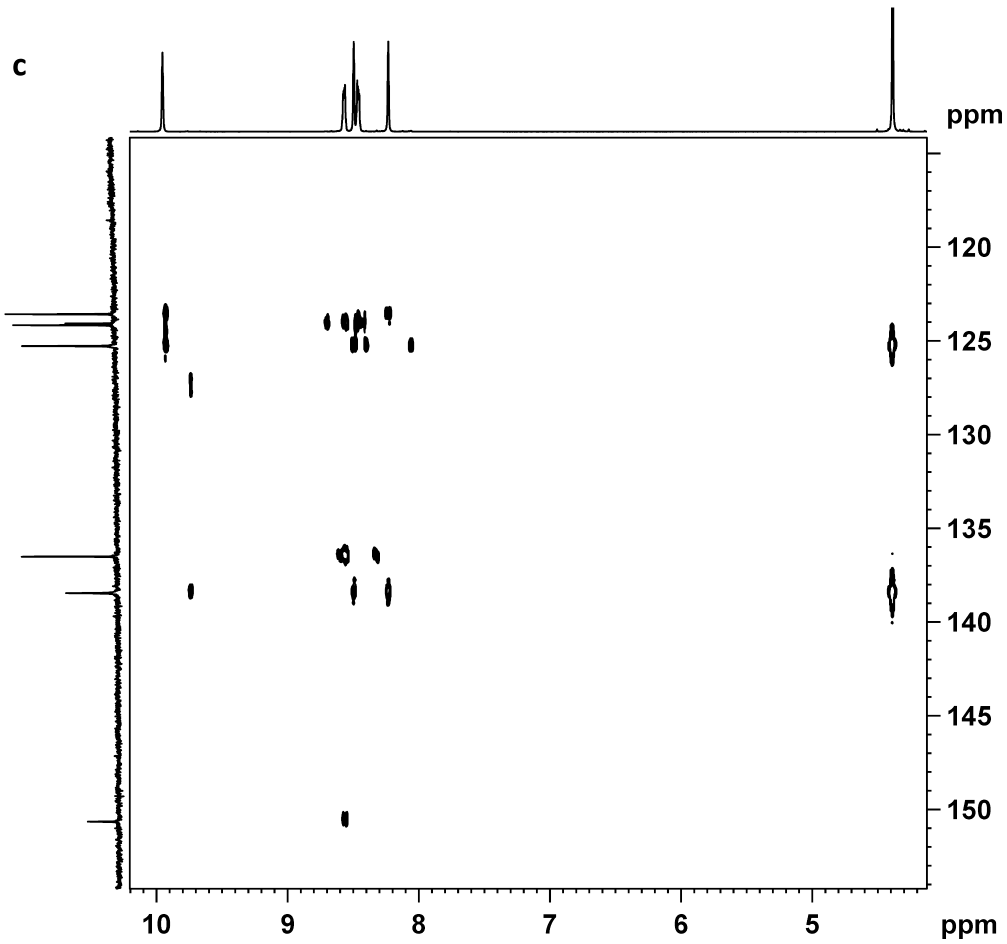

Figure S2. ORTEP plot of the crystal structure for $H_2\mathbf{L1}^{2+}$. Ellipsoids are shown at 50% probability.

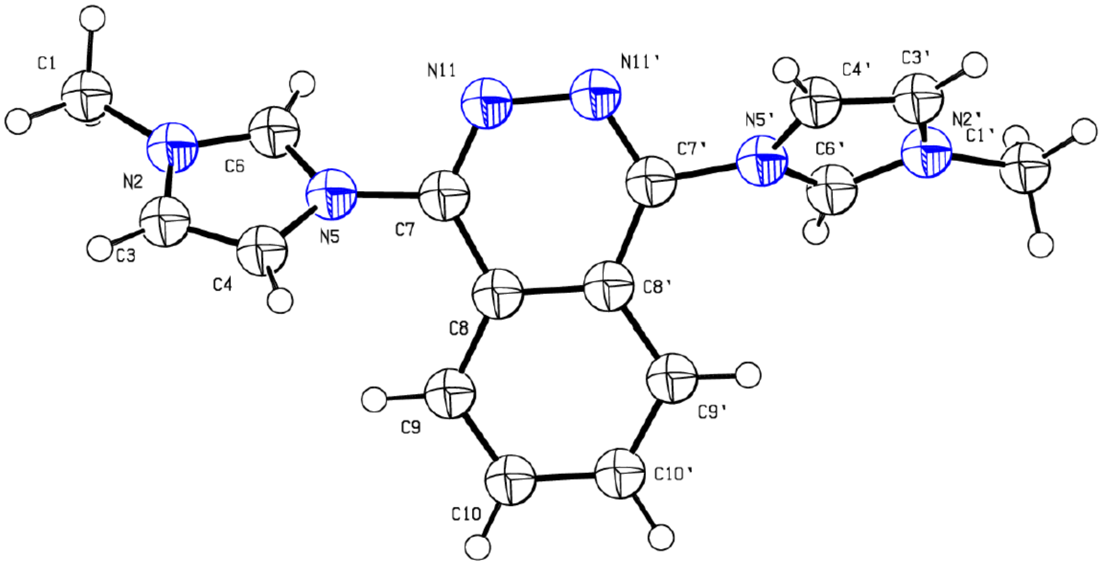

Figure S3. ^{1}H NMR spectrum recorded in acetone-d_6 for the mononuclear Ru complex obtained after reflux of [Ru^{III}(trpy)Cl$_3$] with H_2**L1**$(Cl)_2$ in MeOH.

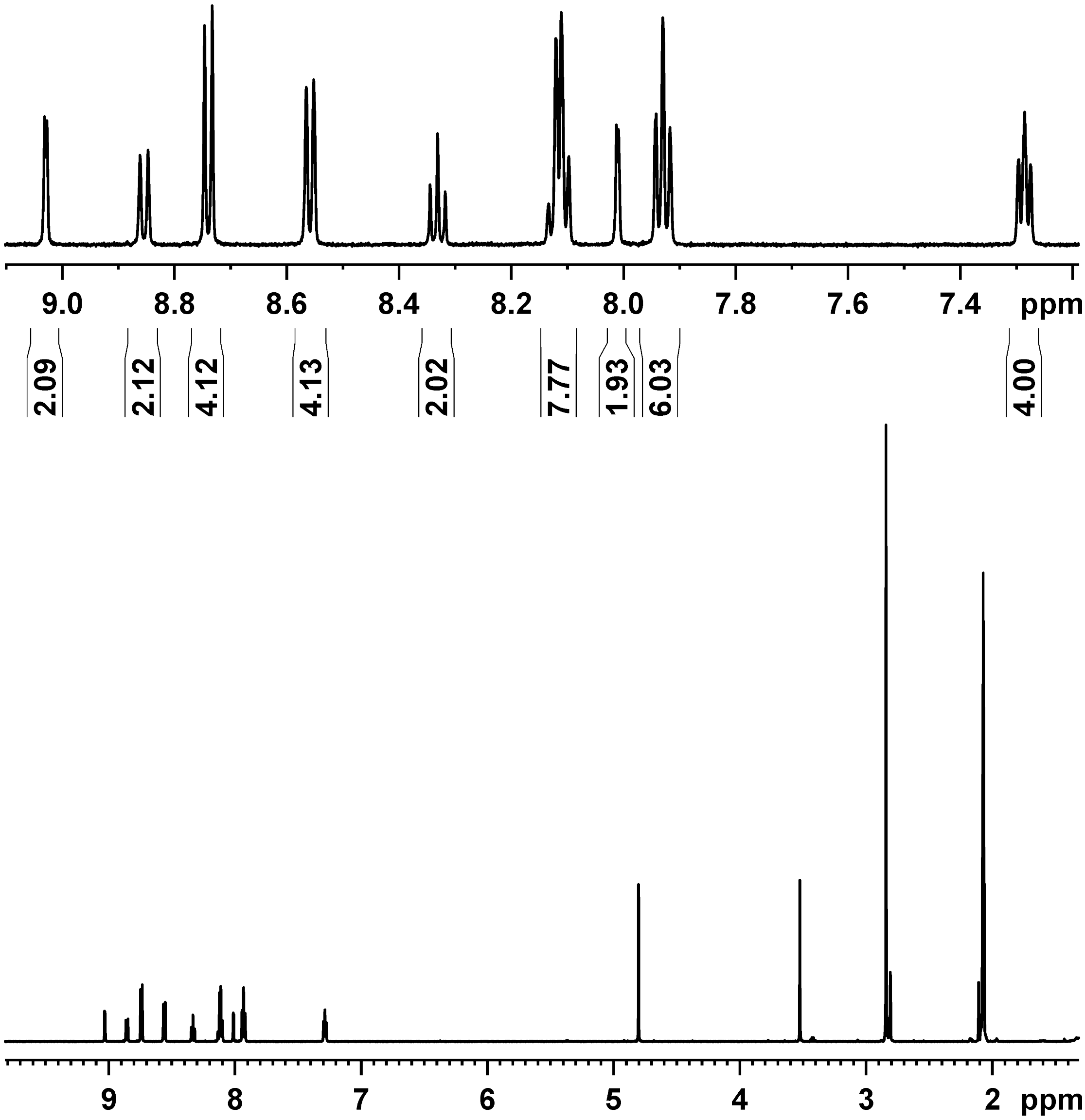

Figure S4. 1D and 2D NMR spectra of **1a**$^+$ (600 MHz, 298K, CD_2Cl_2): a) 1D ^{1}H (aromatic region), b) 1D $^{13}C\{^1H\}$, c) 2D HSQC (aromatic region), d) 2D HMBC (aromatic region), e) 2D ROESY.

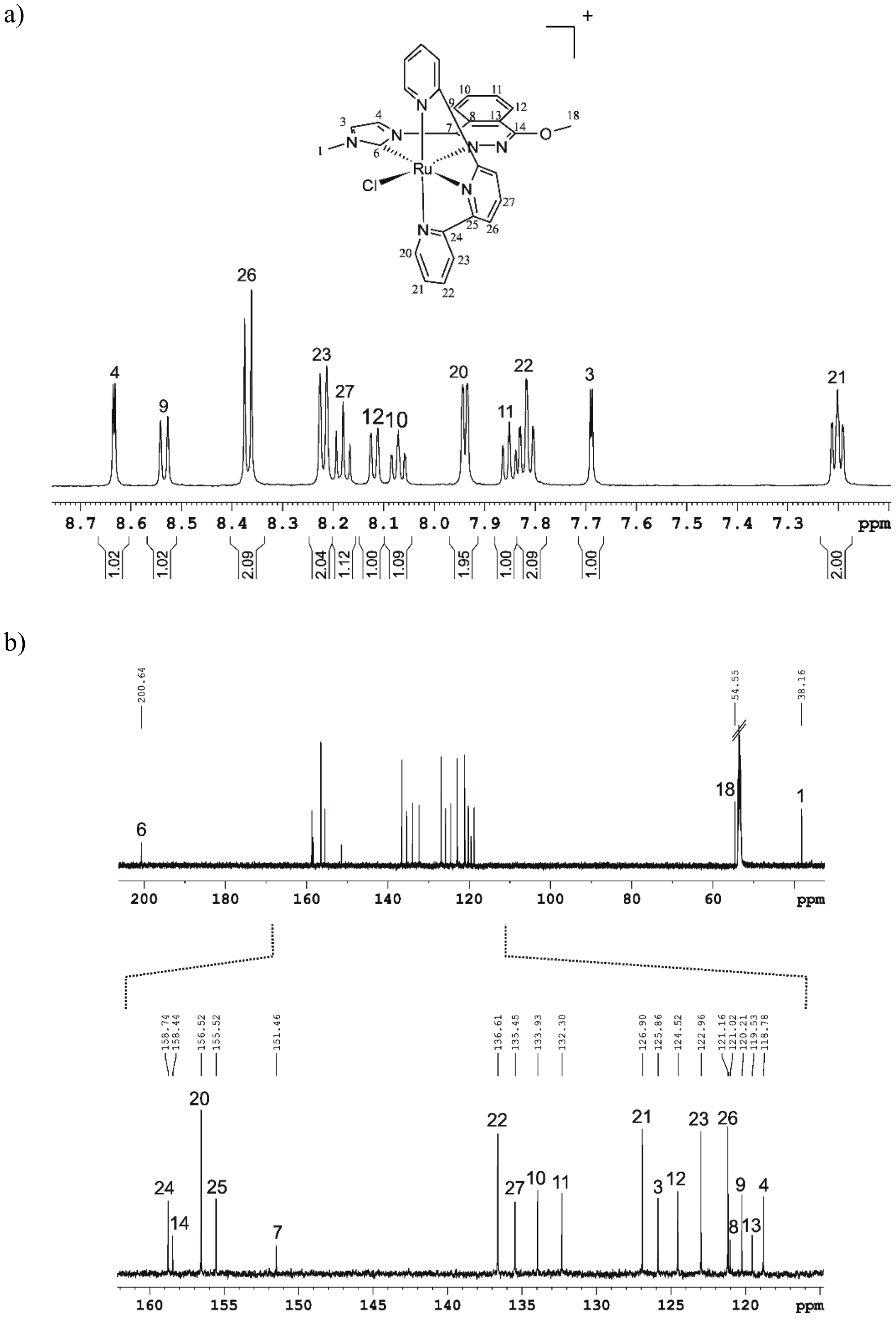

c)

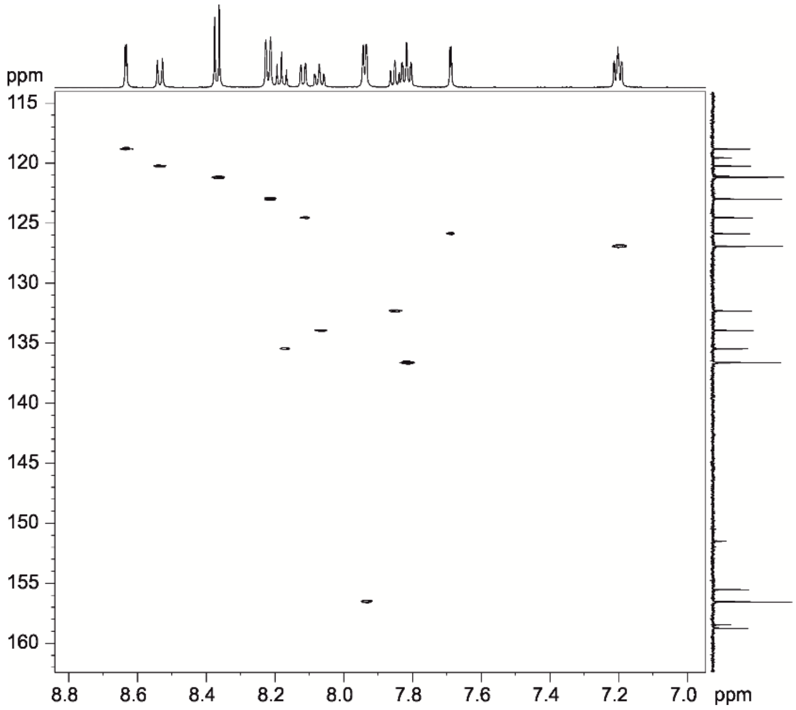
ppm
115
120
125
130
135
140
145
150
155
160
8.8
8.6
8.4
8.2
8.0
7.8
7.6
7.4
7.2
7.0
ppm

d)

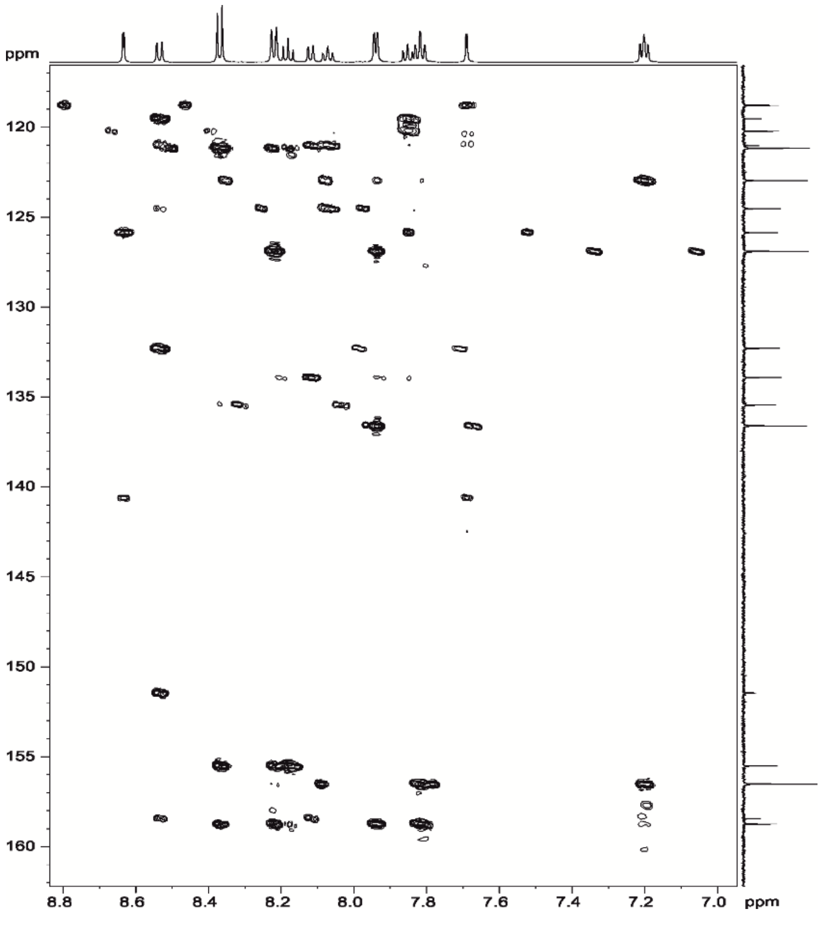
ppm
120
125
130
135
140
145
150
155
160
8.8
8.6
8.4
8.2
8.0
7.8
7.6
7.4
7.2
7.0
ppm

e)

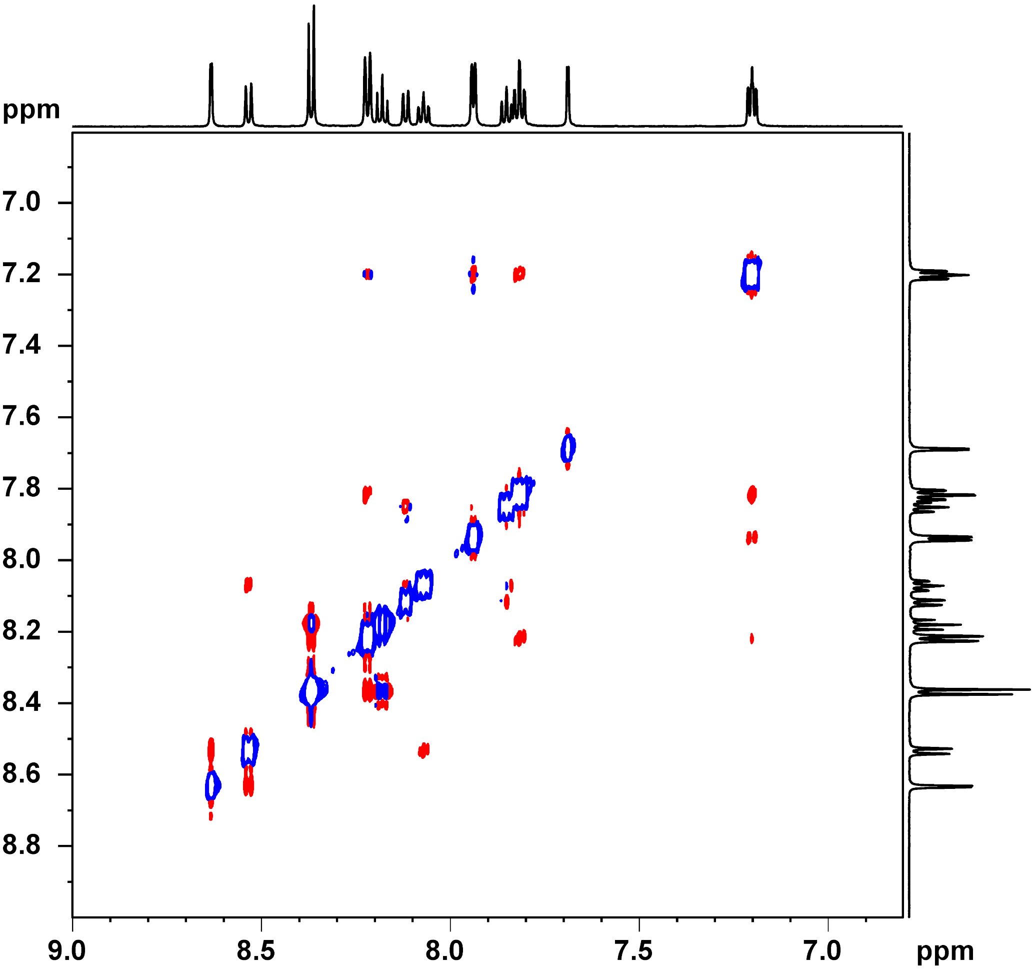

Figure S5. 1D and 2D NMR spectra of **1b**$^+$ (600 MHz, 298K, acetone-d$_6$): a) 1D ^{1}H, b) 1D ^{13}C{^{1}H}, c) 2D HSQC, d) 2D HMBC (aromatic region), e) 2D ROESY (aromatic region), f) 2D TOCSY (aromatic region).

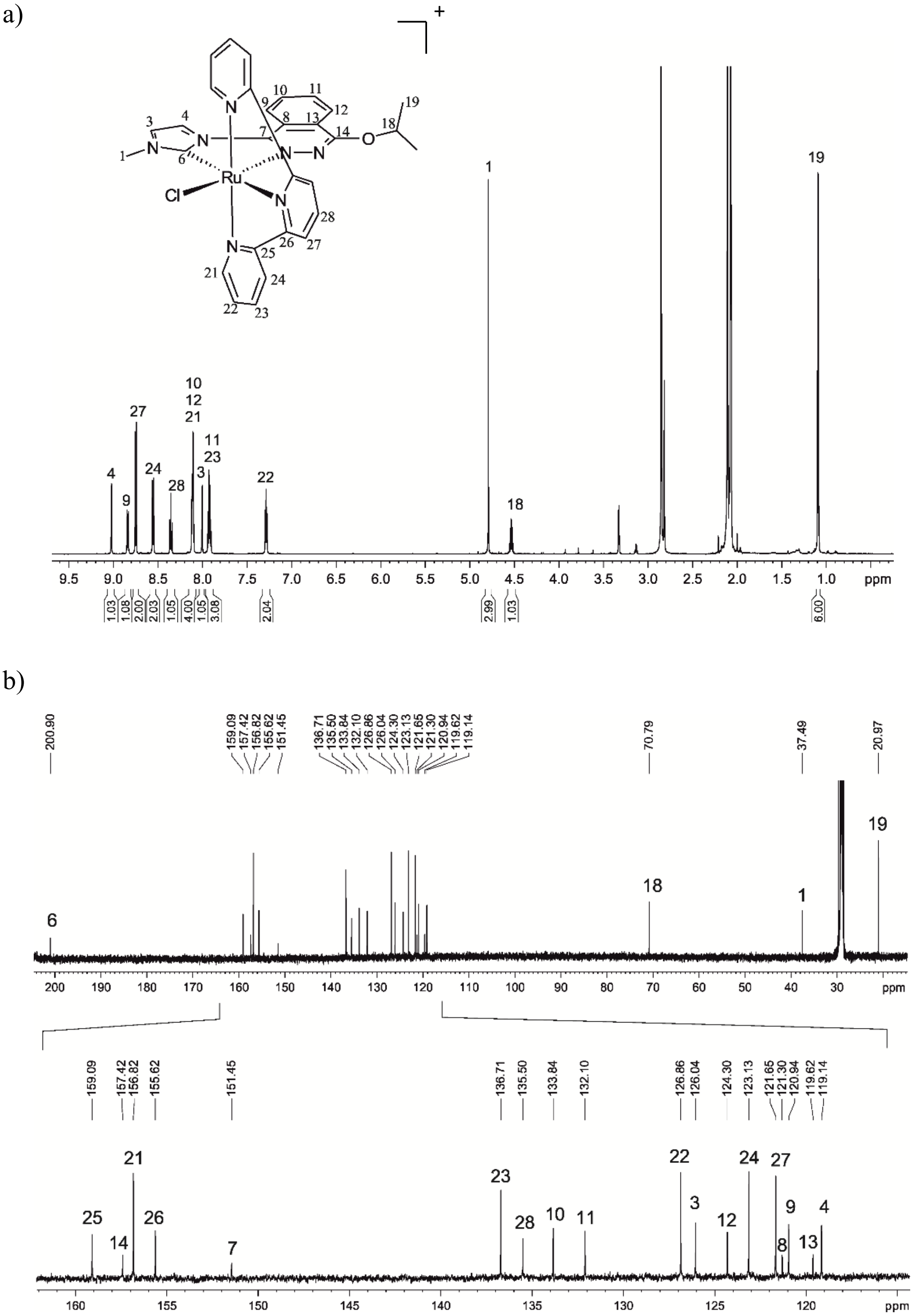

c)

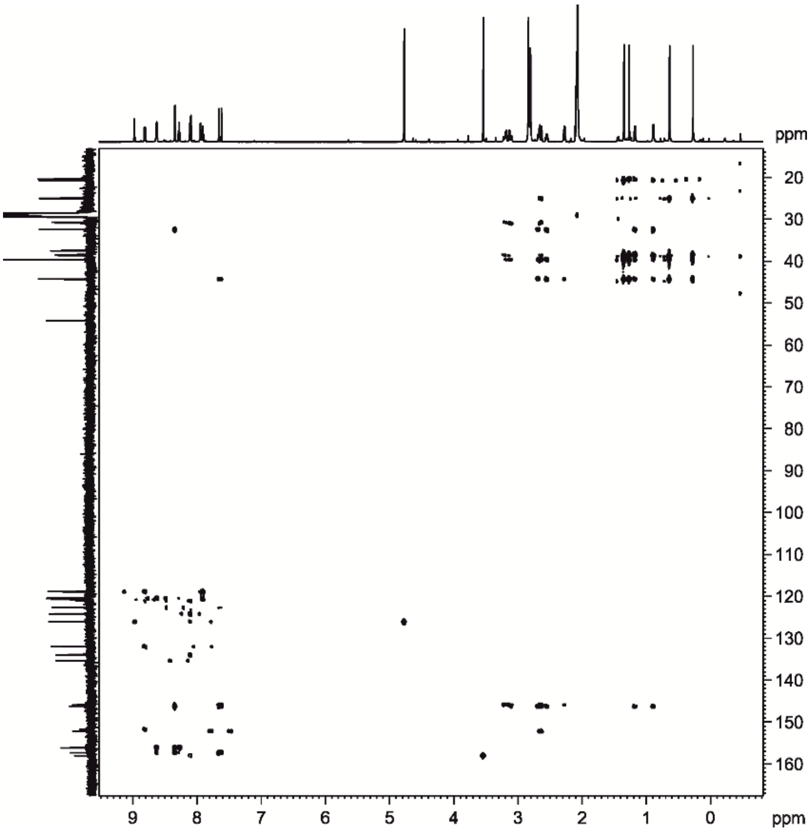

ppm
20
30
40
50
60
70
80
90
100
110
120
130
140
150
160
9
8
7
6
5
4
3
2
1
0
ppm

d)

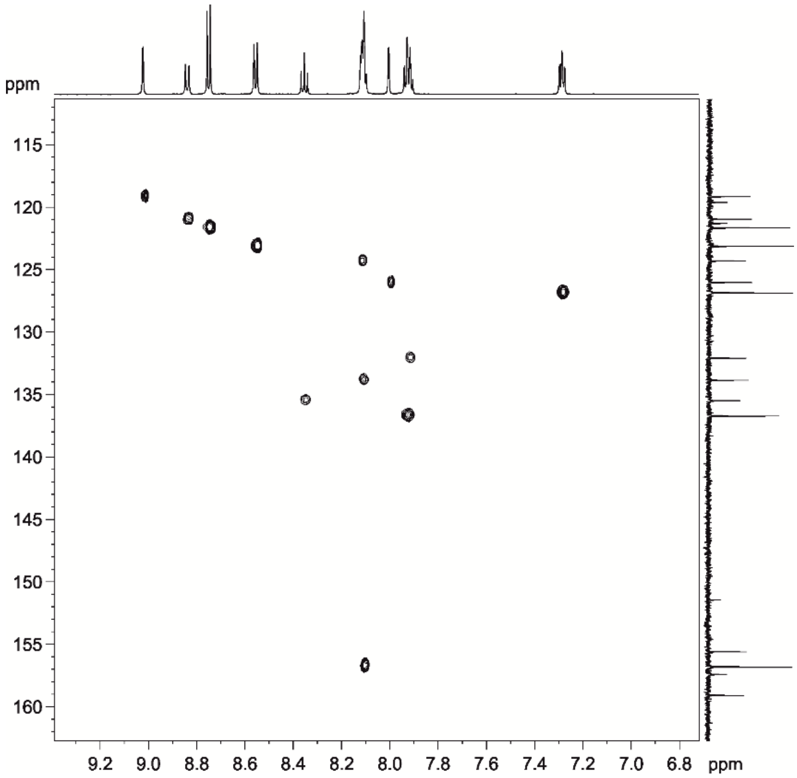

ppm
115
120
125
130
135
140
145
150
155
160
9.2
9.0
8.8
8.6
8.4
8.2
8.0
7.8
7.6
7.4
7.2
7.0
6.8
ppm

e)

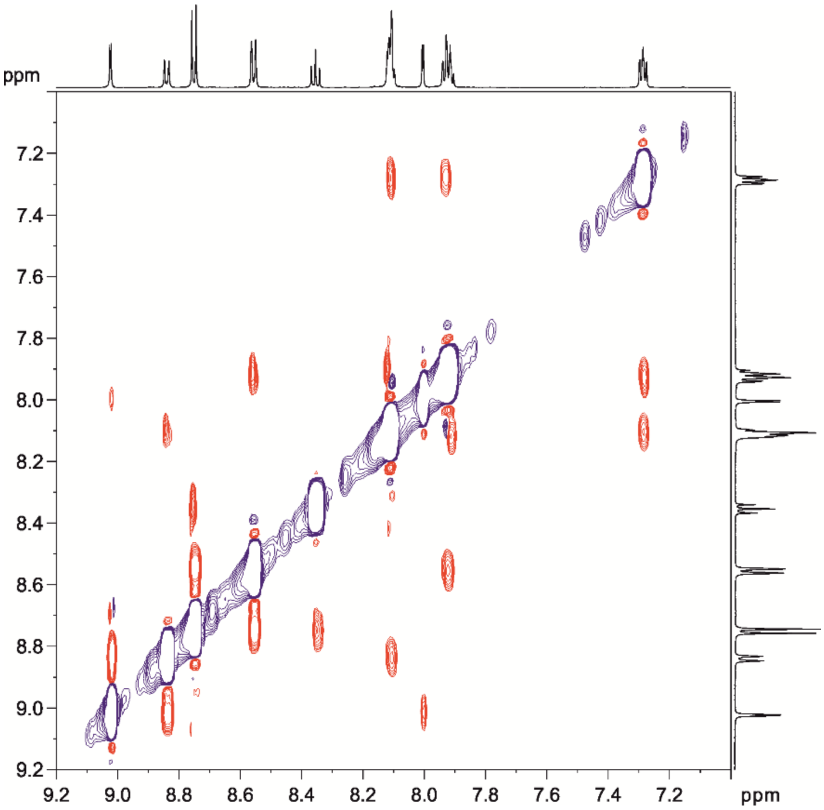
ppm
7.2
7.4
7.6
7.8
8.0
8.2
8.4
8.6
8.8
9.0
9.2
9.2
9.0
8.8
8.6
8.4
8.2
8.0
7.8
7.6
7.4
7.2
ppm

f)

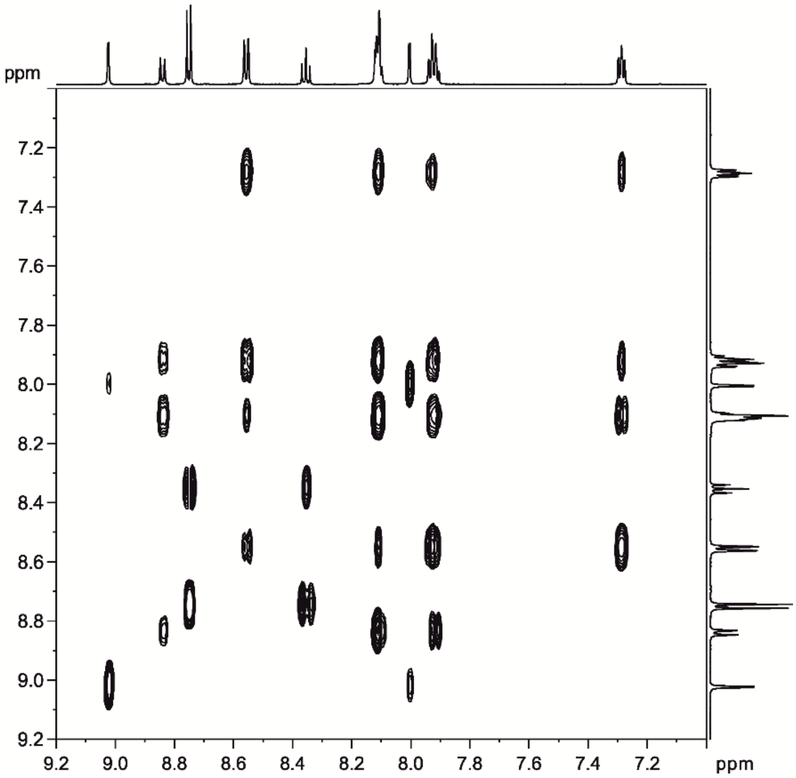
ppm
7.2
7.4
7.6
7.8
8.0
8.2
8.4
8.6
8.8
9.0
9.2
9.2
9.0
8.8
8.6
8.4
8.2
8.0
7.8
7.6
7.4
7.2
ppm

Figure S6. 1D and 2D NMR spectra of **3**$^+$ (600 MHz, 298K, acetone-d$_6$): a) 1D ^{1}H, b) 1D ^{13}C{^{1}H}, c) 2D HSQC, d) 2D HMBC, e) 2D ROESY, f) 2D TOCSY.

a)

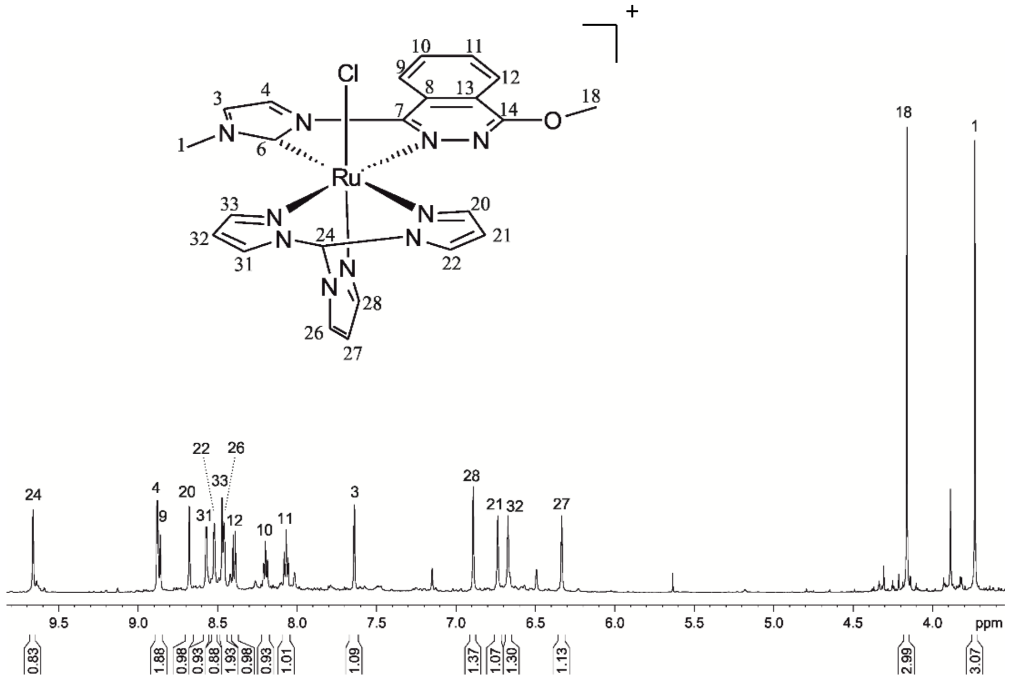

b)

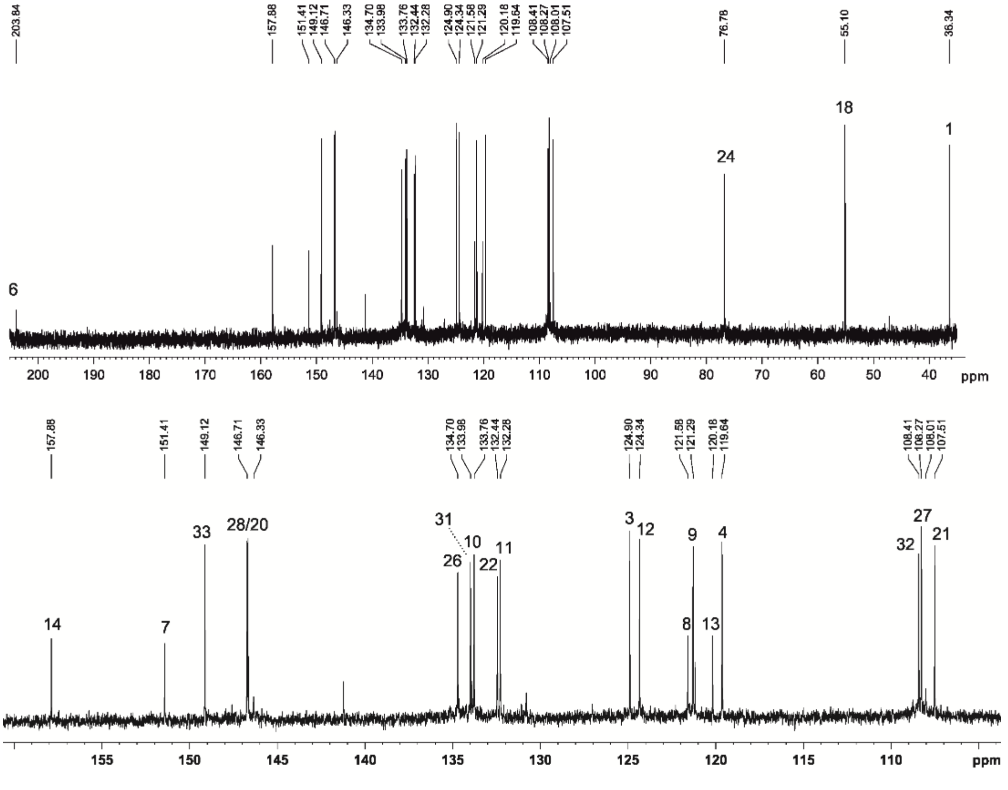

c)

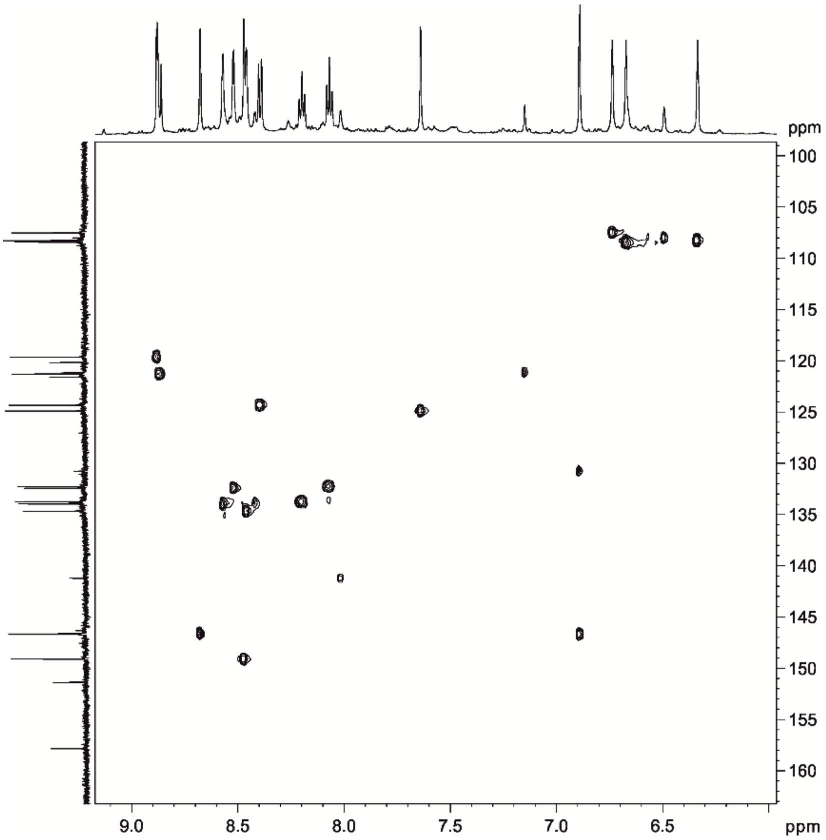
ppm
100
105
110
115
120
125
130
135
140
145
150
155
160
9.0
8.5
8.0
7.5
7.0
6.5
ppm

d)

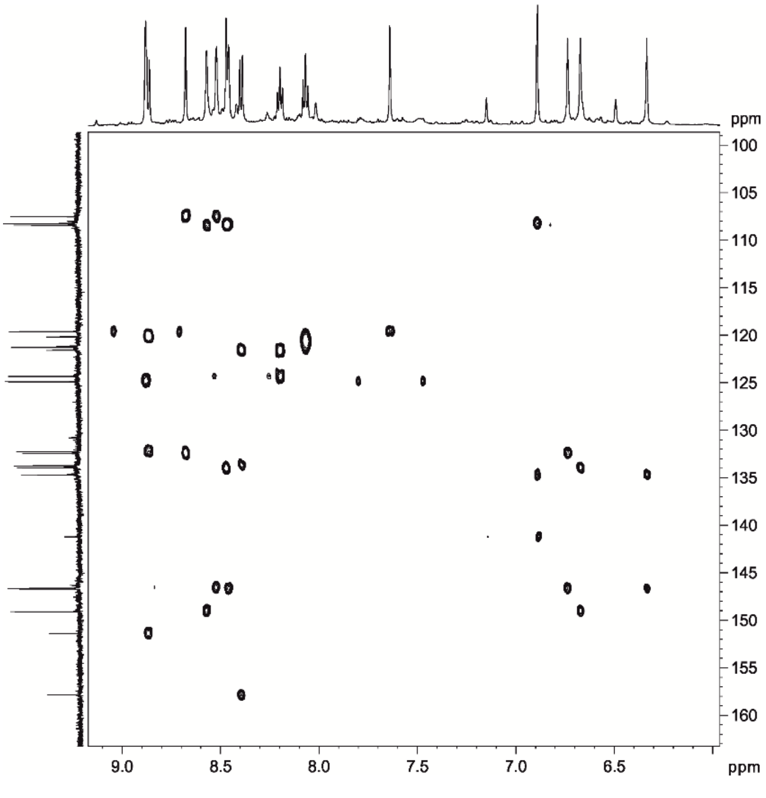
ppm
100
105
110
115
120
125
130
135
140
145
150
155
160
9.0
8.5
8.0
7.5
7.0
6.5
ppm

e)

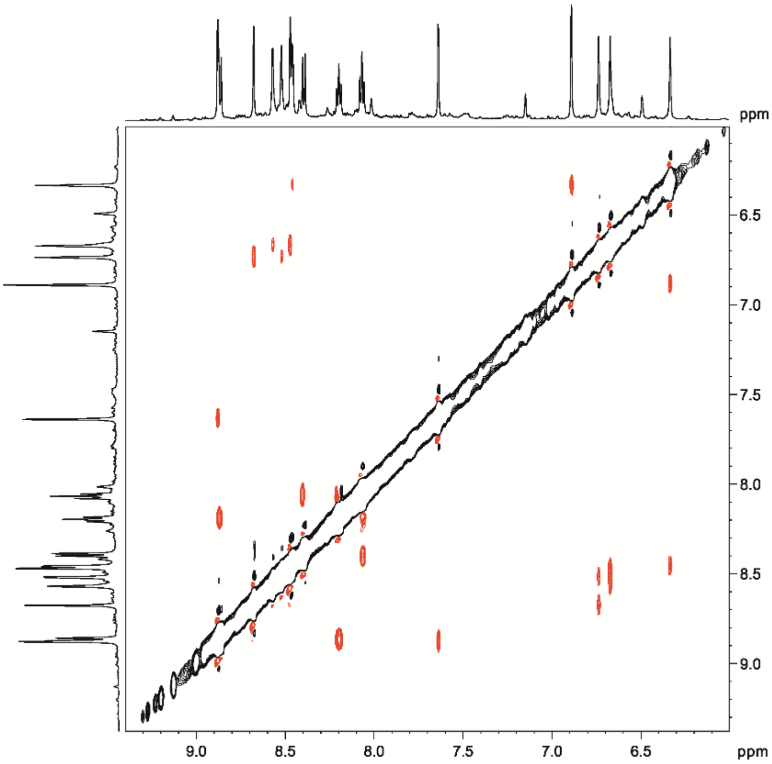
ppm
6.5
7.0
7.5
8.0
8.5
9.0
9.0
8.5
8.0
7.5
7.0
6.5
ppm

f)

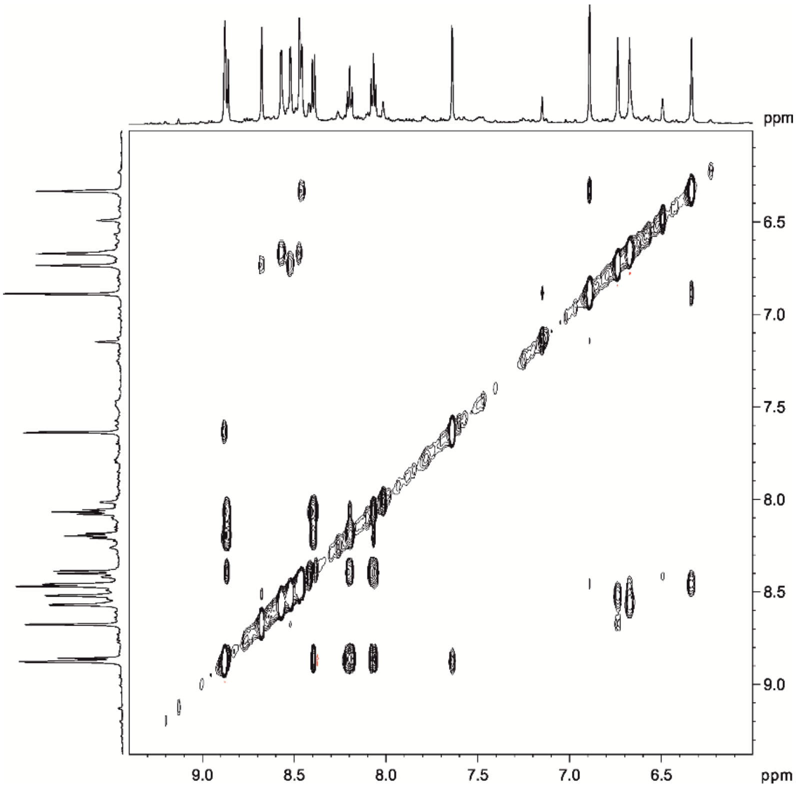
ppm
6.5
7.0
7.5
8.0
8.5
9.0
9.0
8.5
8.0
7.5
7.0
6.5
ppm

Figure S7. 1D and 2D NMR spectra of **5**$^+$ (600 MHz, 298K, acetone-d$_6$): a) 1D ^{1}H (aromatic region), b) 1D ^{13}C{^{1}H}, c) 2D HSQC, d) 2D ROESY, e) 1D selective NOESY.

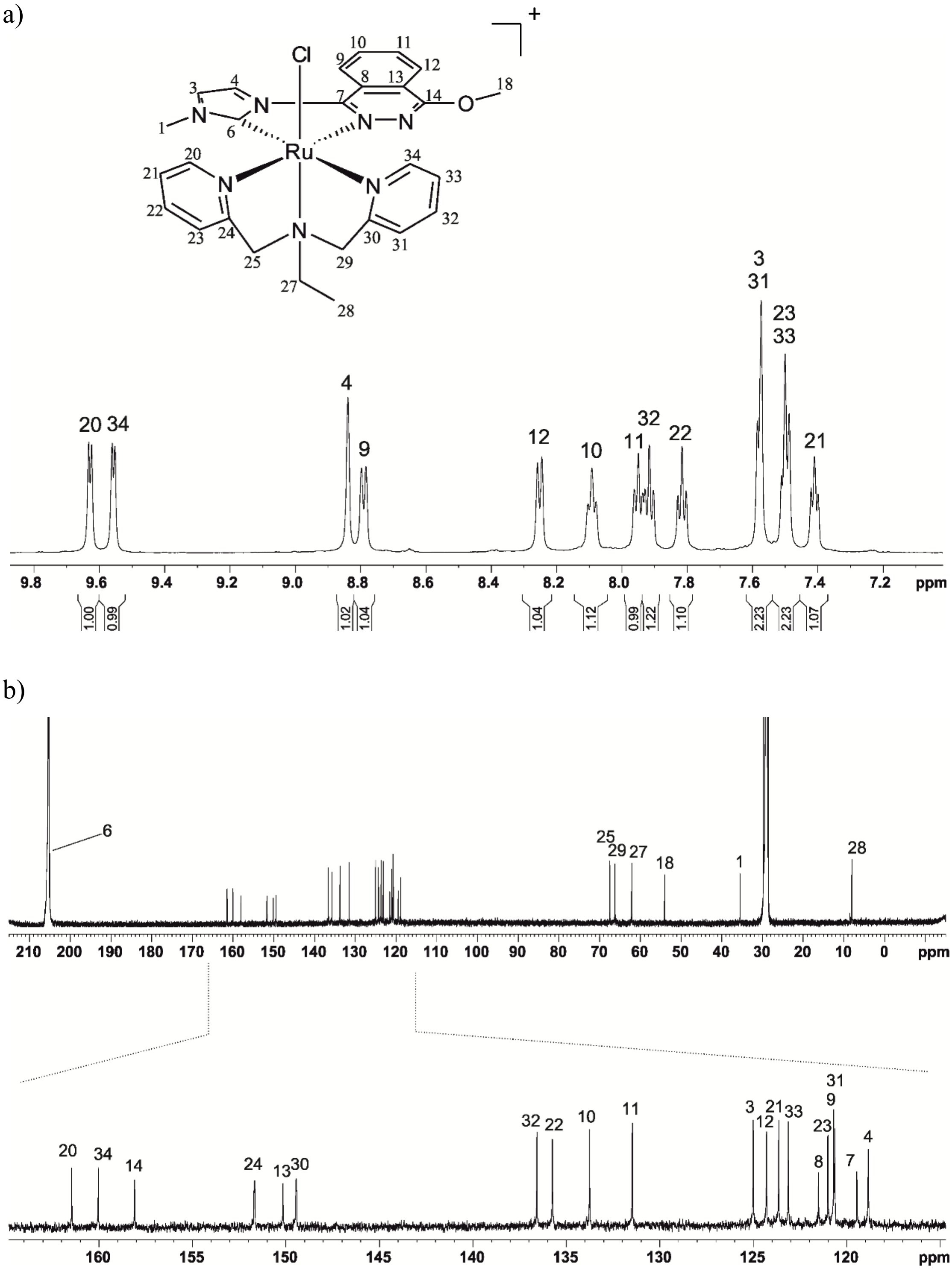

c)

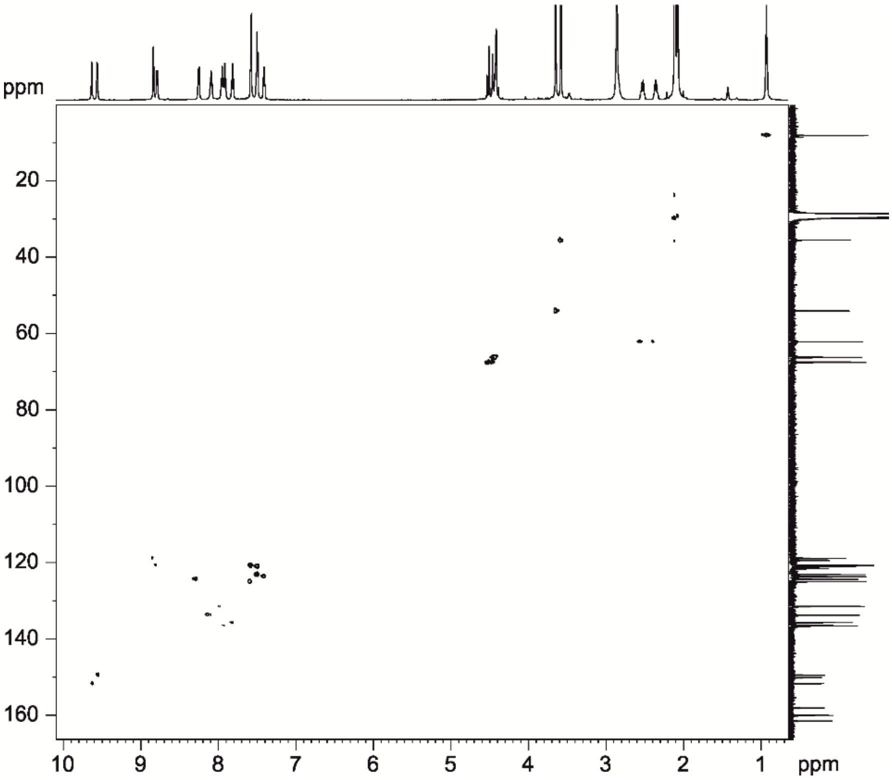
ppm
20
40
60
80
100
120
140
160
10
9
8
7
6
5
4
3
2
1
ppm

d)

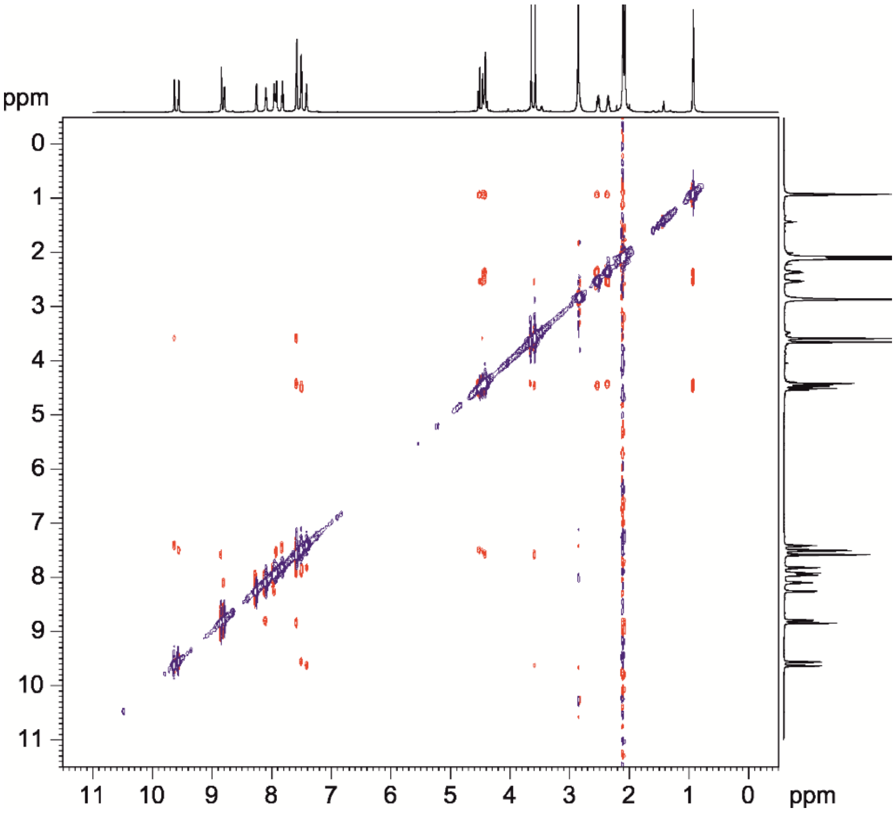
ppm
0
1
2
3
4
5
6
7
8
9
10
11
11
10
9
8
7
6
5
4
3
2
1
0
ppm

e)

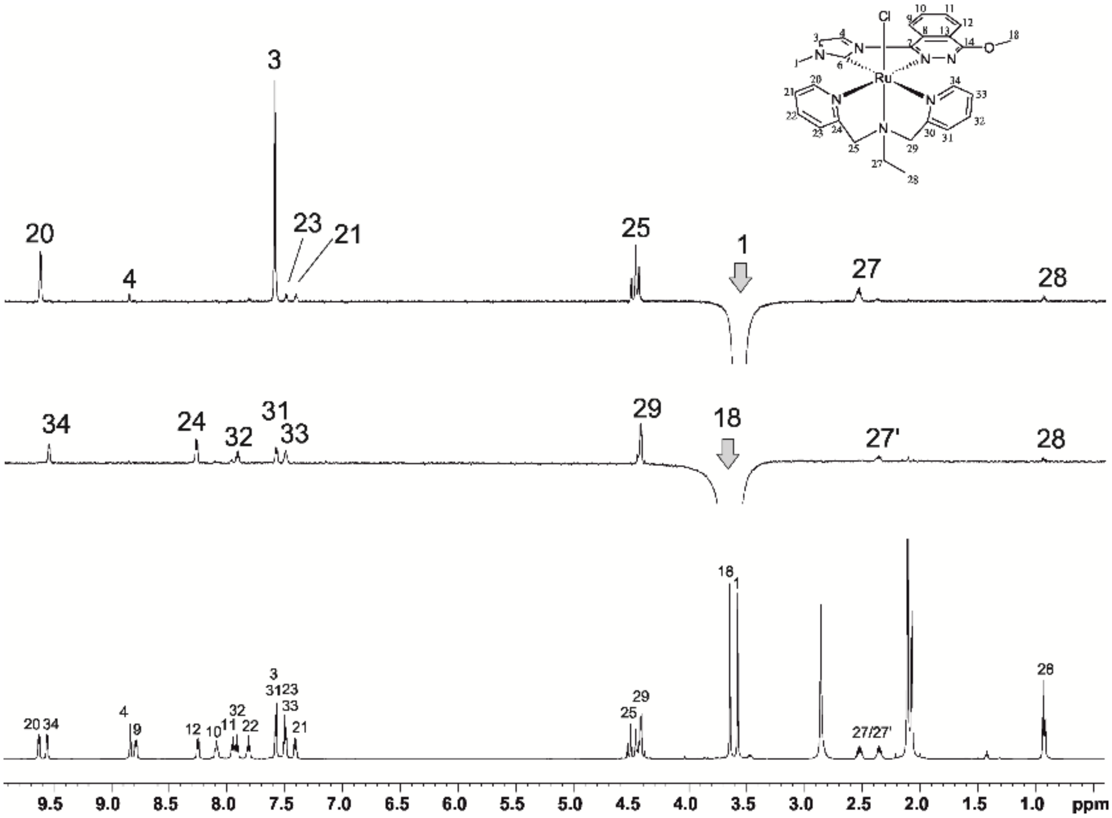
Cl
Ru
N
O
1
3
4
6
7
8
9
10
11
12
13
14
18
20
21
22
23
24
25
27
28
29
30
31
32
33
34
20
4
3
23
21
25
1
27
28
34
24
32
31
33
29
18
27'
28
20 34
4
9
12
10
11
32
22
3
31
23
33
21
25
29
18
1
27/27'
28
9.5
9.0
8.5
8.0
7.5
7.0
6.5
6.0
5.5
5.0
4.5
4.0
3.5
3.0
2.5
2.0
1.5
1.0
ppm

Figure S8. ESI-MS spectra of **1a**$^+$ (a), **1b**$^+$ (b), **3**$^+$ (c) and **5**$^+$ (d).

a)

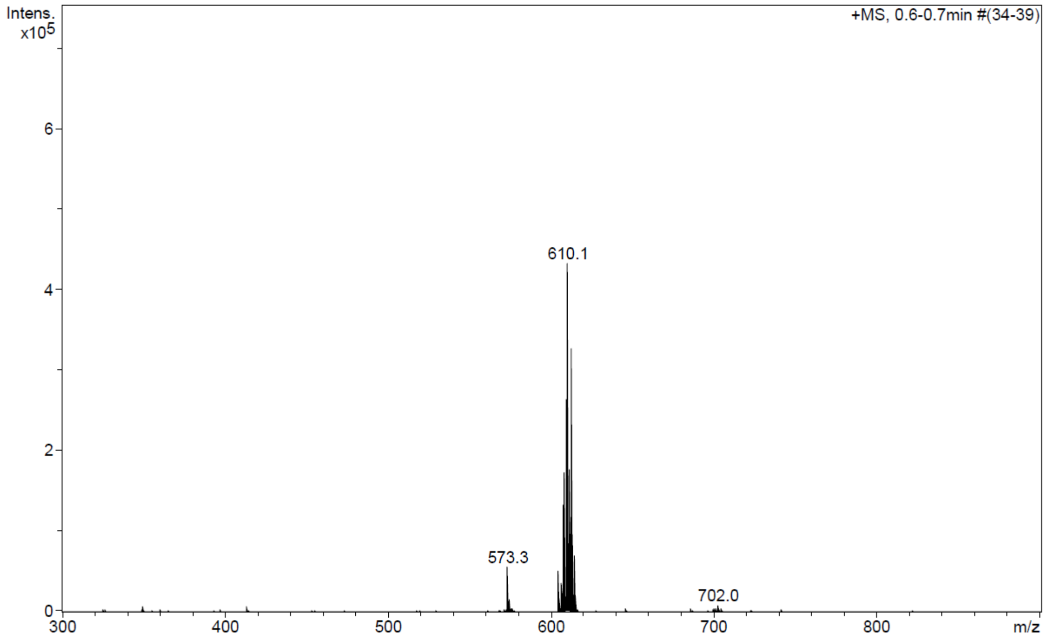

b)

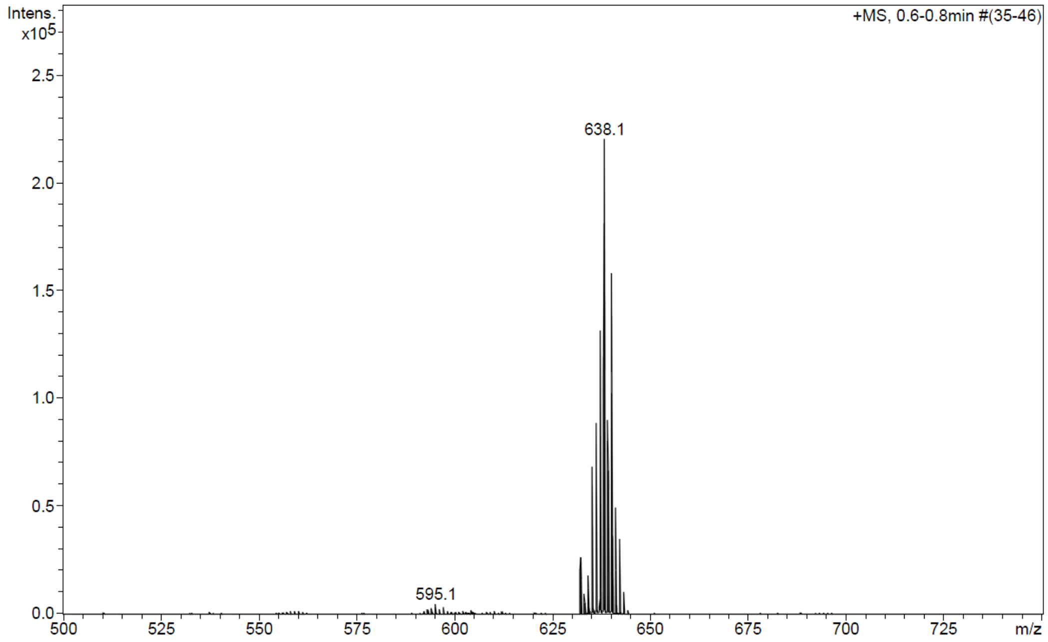

c)

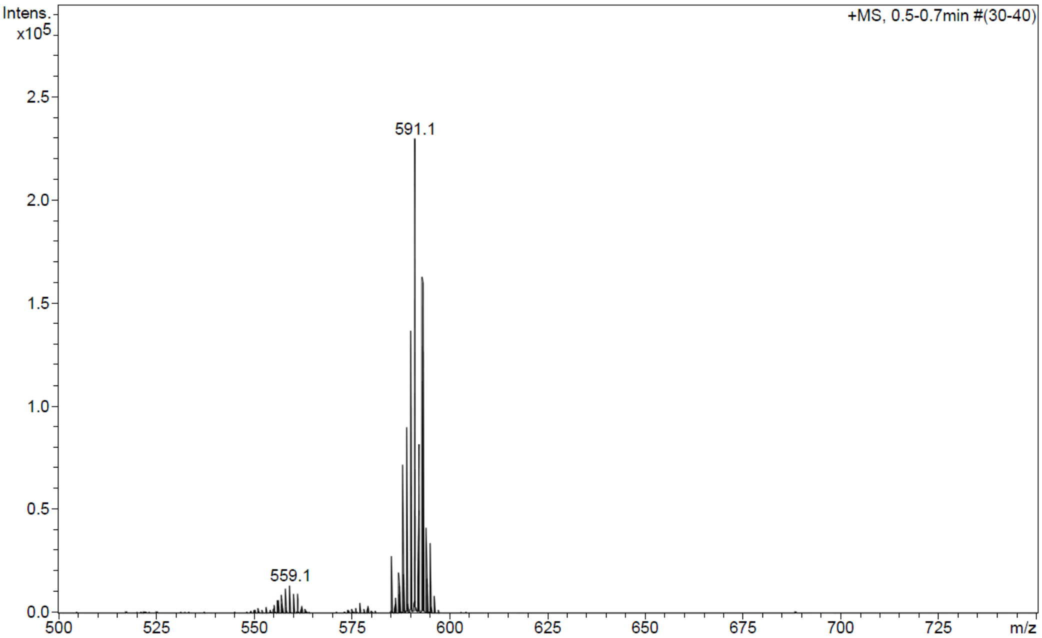
Intens.
x10^5
2.5
2.0
1.5
1.0
0.5
0.0
+MS, 0.5-0.7min #(30-40)
591.1
559.1
500
525
550
575
600
625
650
675
700
725
m/z

d)

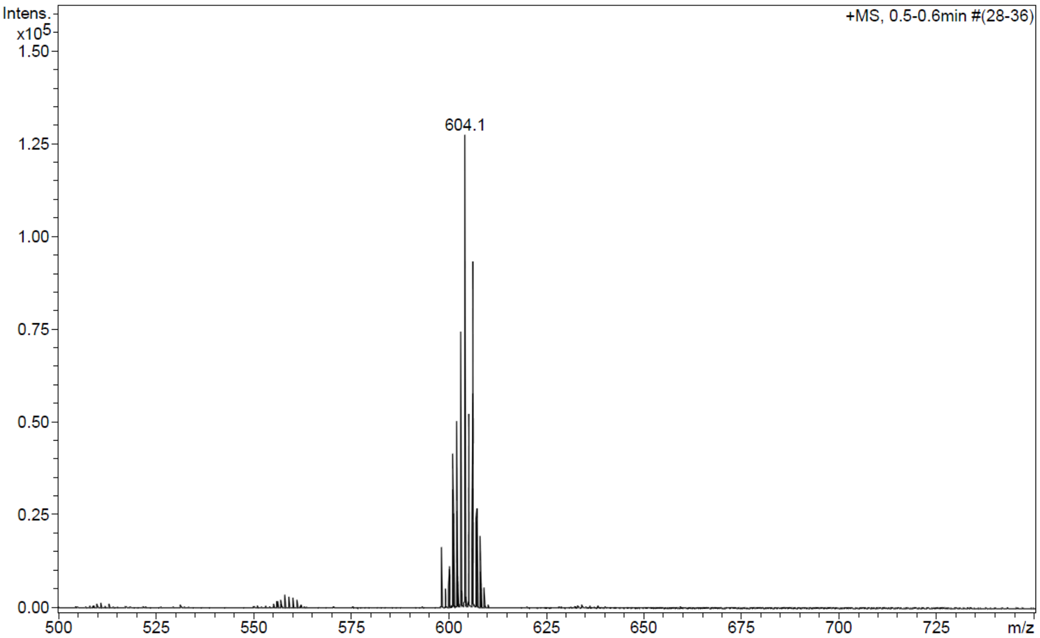
Intens.
x10^5
1.50
1.25
1.00
0.75
0.50
0.25
0.00
+MS, 0.5-0.6min #(28-36)
604.1
500
525
550
575
600
625
650
675
700
725
m/z

Figure S9. ORTEP plot of the cationic moiety of **5**(PF_6) (a) and its unit cell (b). Ellipsoids are shown at 50% probability.

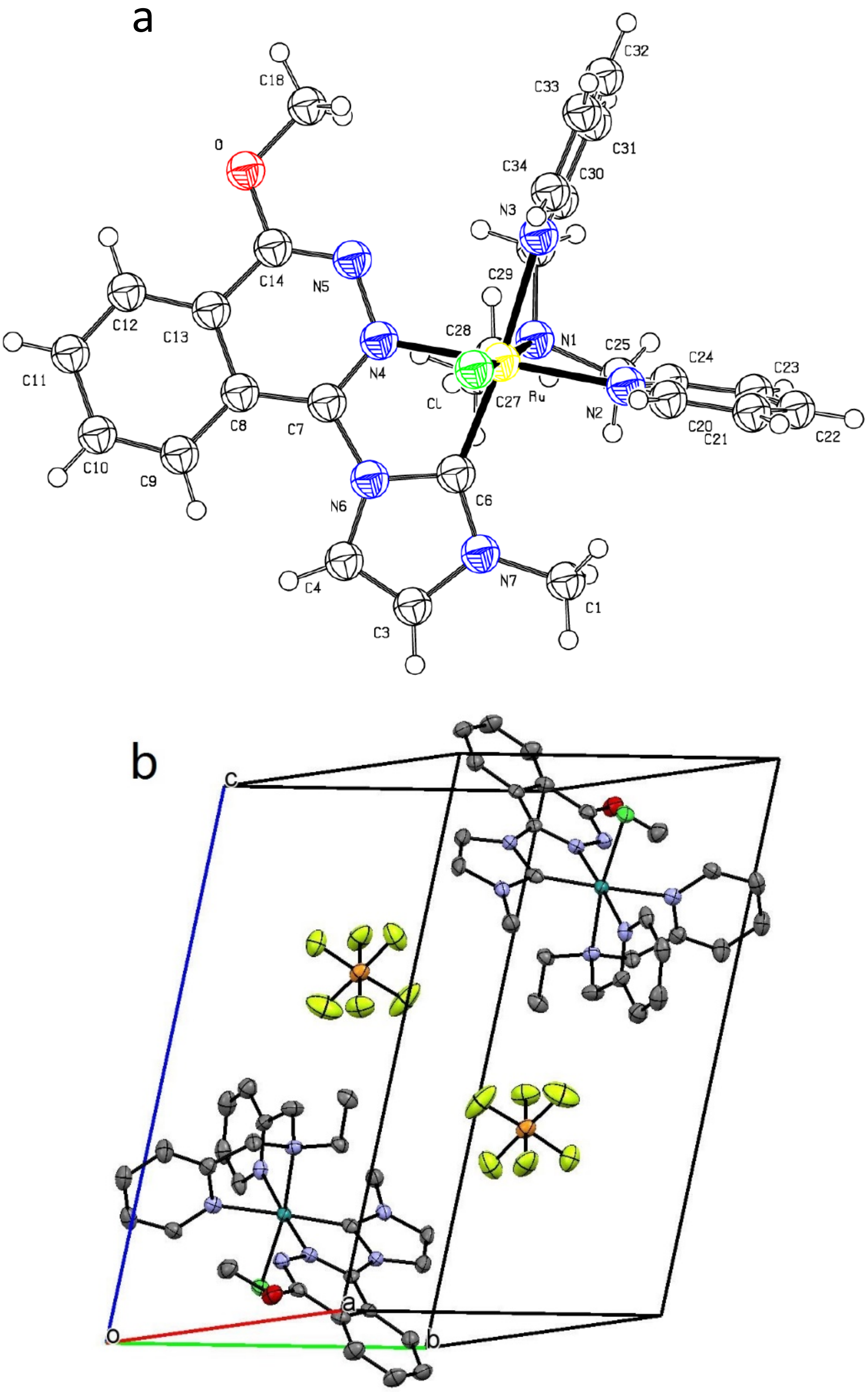

Figure S10. Aromatic region of the ^{1}H NMR spectra of **1a**$^{+}$ (a) and **2a**$^{2+}$ (b) in acetone-d$_6$ and its corresponding proton assignment. Red arrows show down-field shifts and blue arrows up-field shifts.

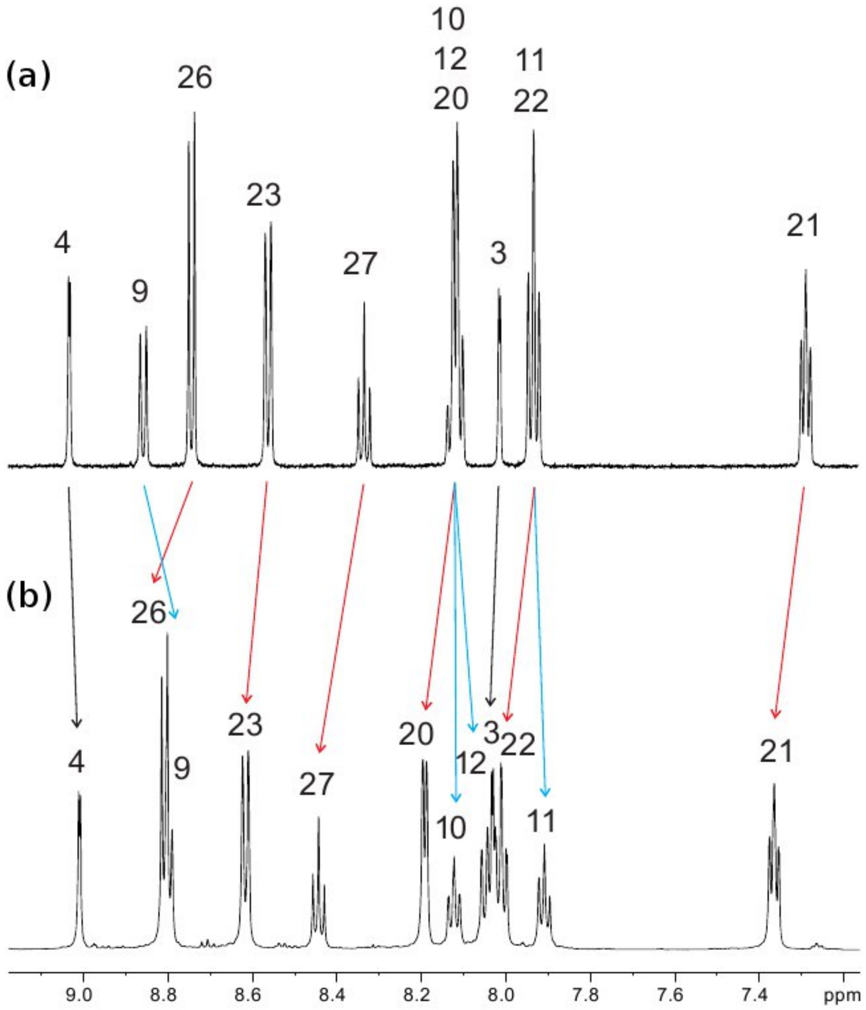

Figure S11. 1D and 2D NMR spectra of **2a**$^{2+}$ (600 MHz, 298K, acetone-d_6): a) 1D ^{1}H, b) 1D ^{13}C{^{1}H}, c) 2D HSQC, d) 2D HMBC.

a)

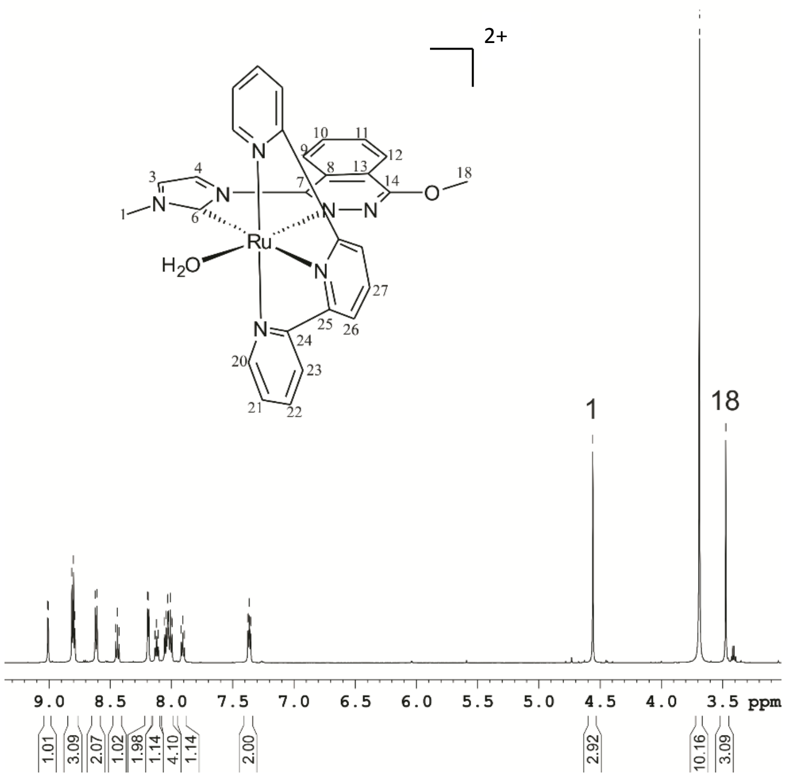

b)

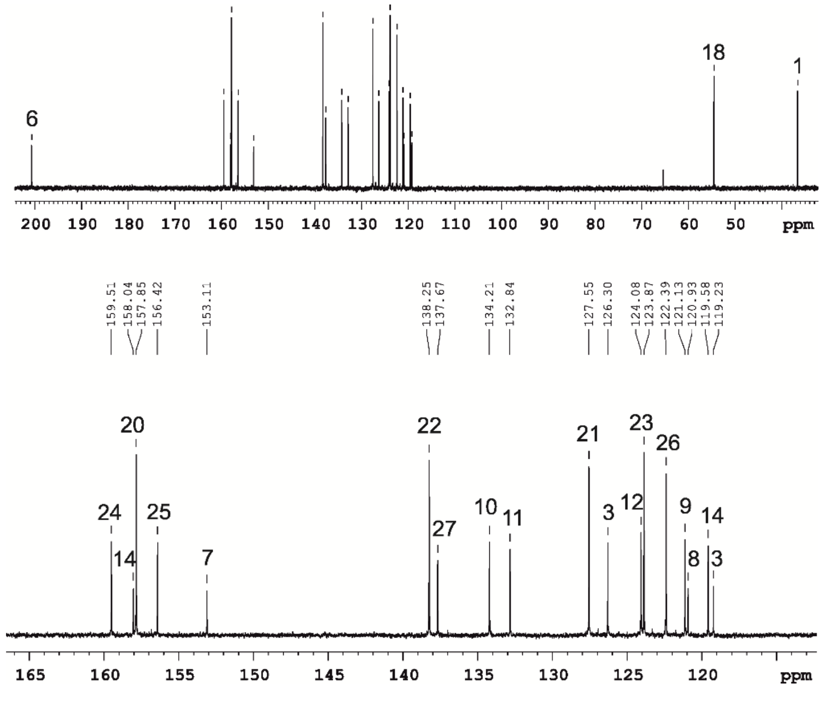

c)

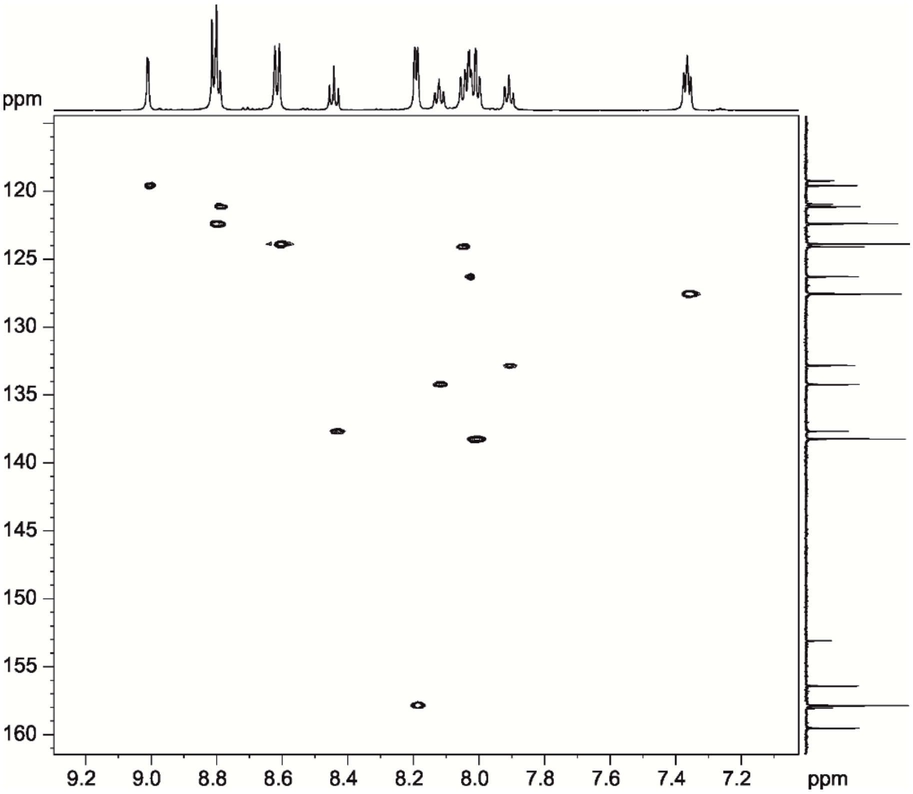
ppm
120
125
130
135
140
145
150
155
160
9.2
9.0
8.8
8.6
8.4
8.2
8.0
7.8
7.6
7.4
7.2
ppm

d)

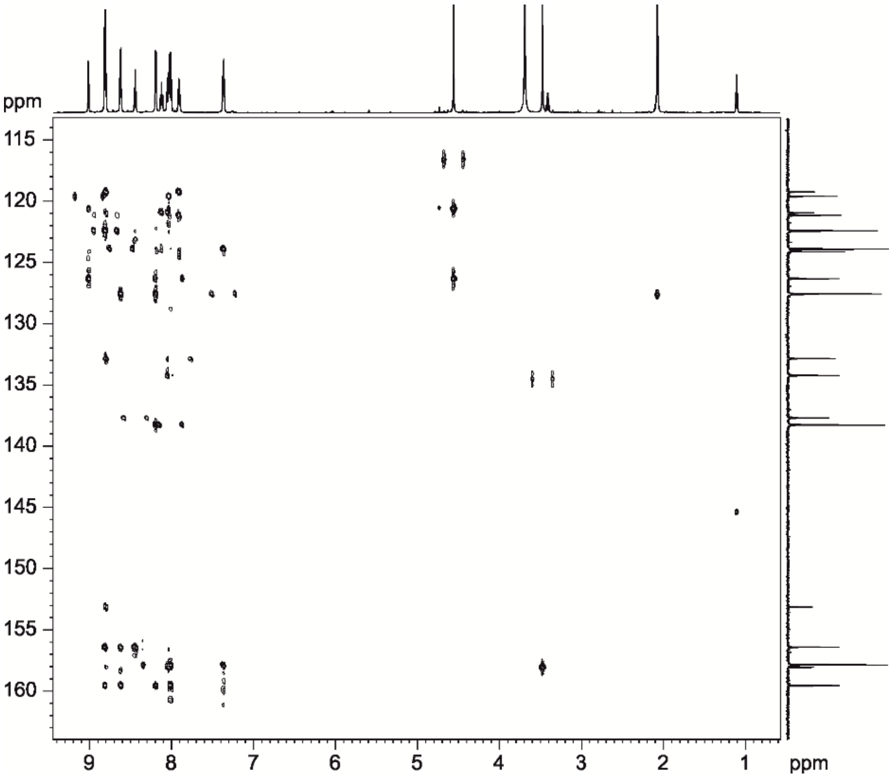
ppm
115
120
125
130
135
140
145
150
155
160
9
8
7
6
5
4
3
2
1
ppm

Figure S12. 1D and 2D NMR spectra of **2b**$^{2+}$ (600 MHz, 298K, acetone-d$_6$): a) 1D ^{1}H, b) 1D ^{13}C{^{1}H}, c) 2D HSQC, d) 2D HMBC, e) 2D ROESY, f) 2D TOCSY.

a)

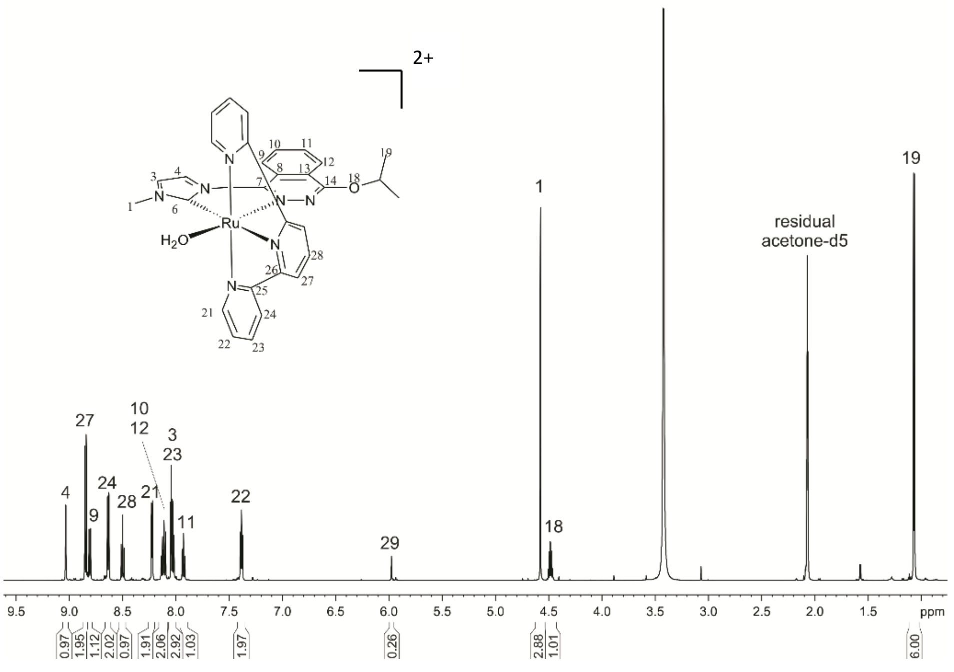

b)

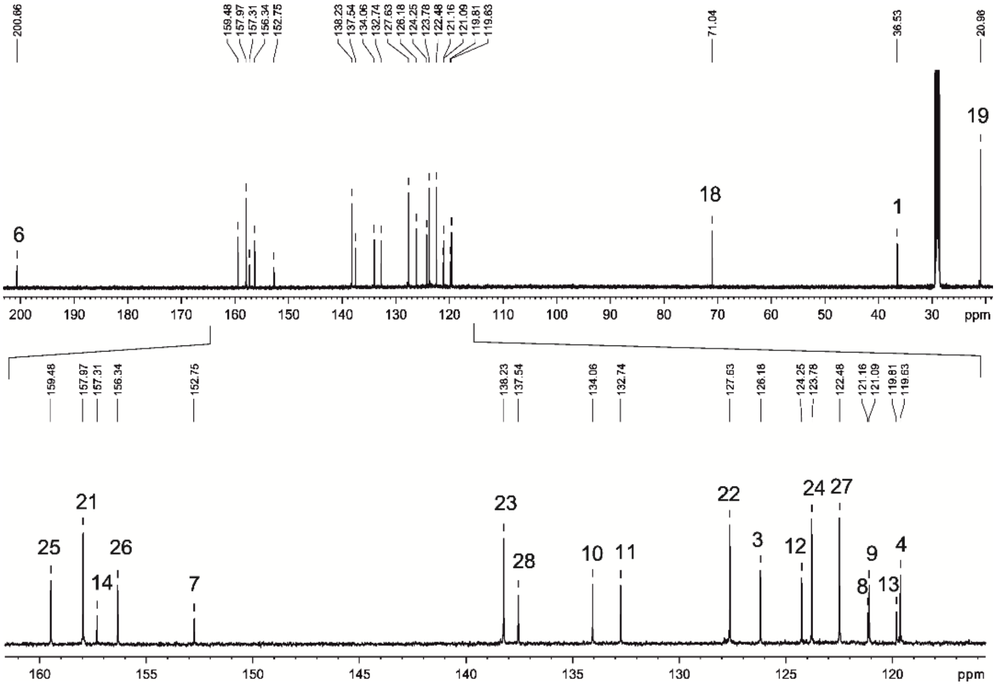

c)

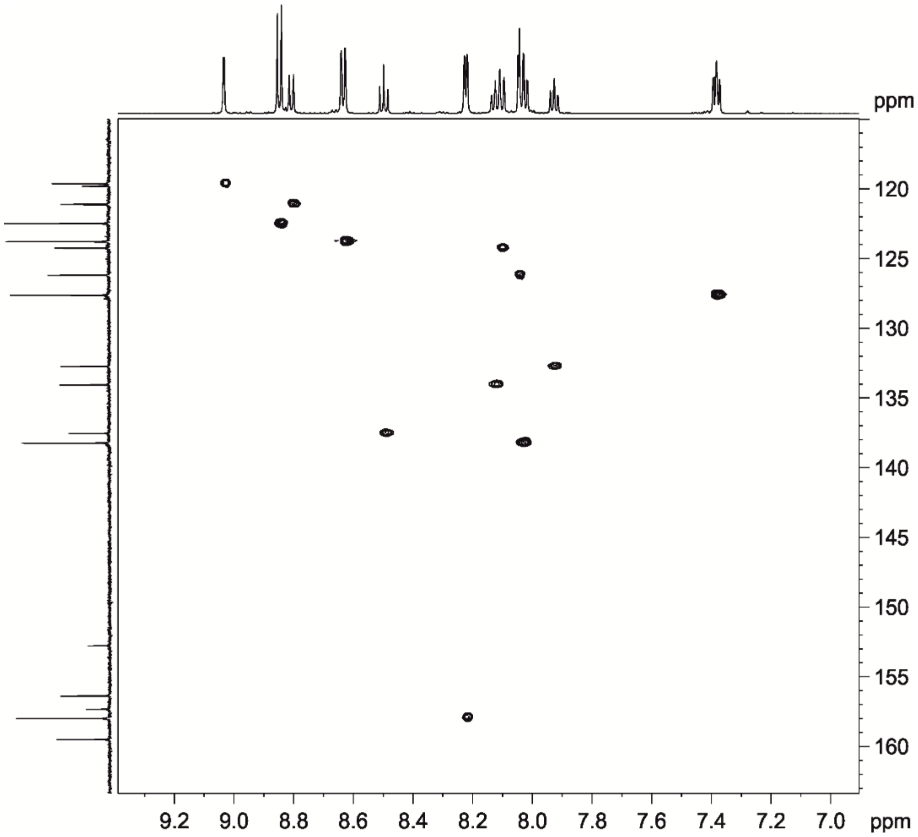
ppm
120
125
130
135
140
145
150
155
160
9.2
9.0
8.8
8.6
8.4
8.2
8.0
7.8
7.6
7.4
7.2
7.0
ppm

d)

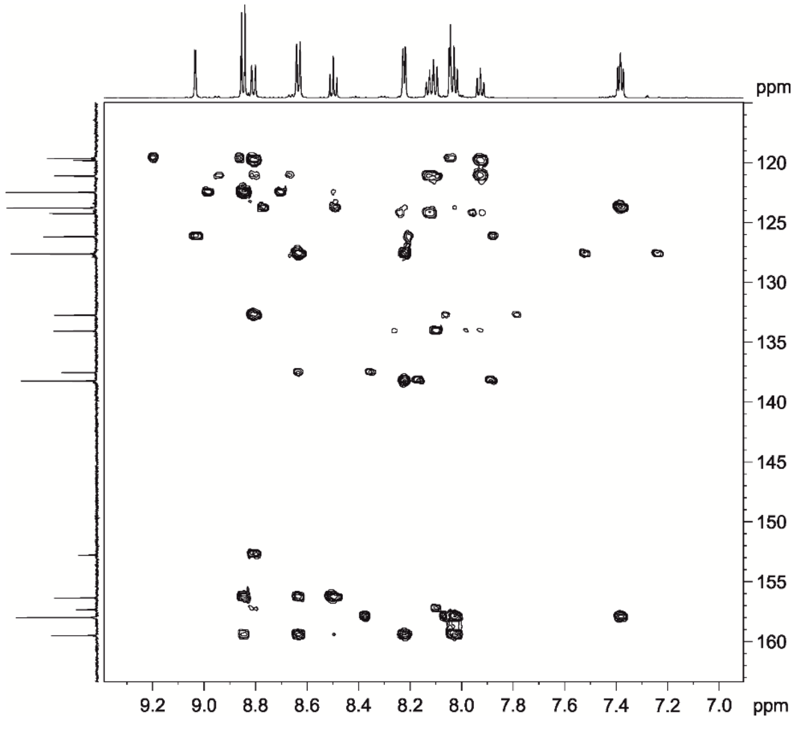
ppm
120
125
130
135
140
145
150
155
160
9.2
9.0
8.8
8.6
8.4
8.2
8.0
7.8
7.6
7.4
7.2
7.0
ppm

e)

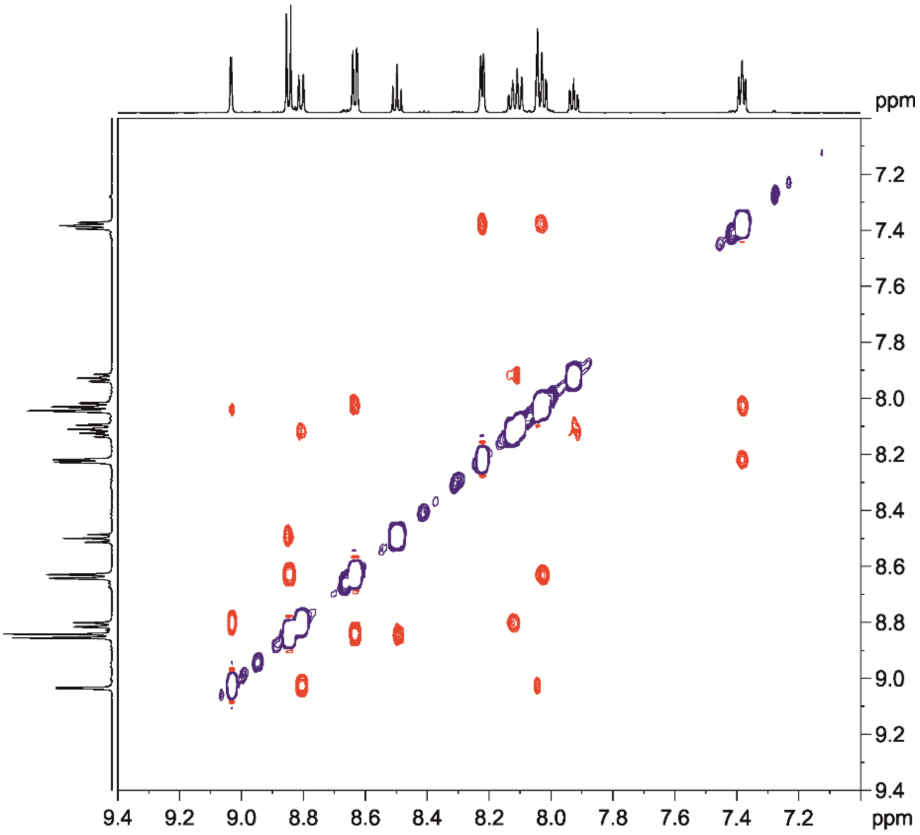
ppm
7.2
7.4
7.6
7.8
8.0
8.2
8.4
8.6
8.8
9.0
9.2
9.4
9.4
9.2
9.0
8.8
8.6
8.4
8.2
8.0
7.8
7.6
7.4
7.2
ppm

f)

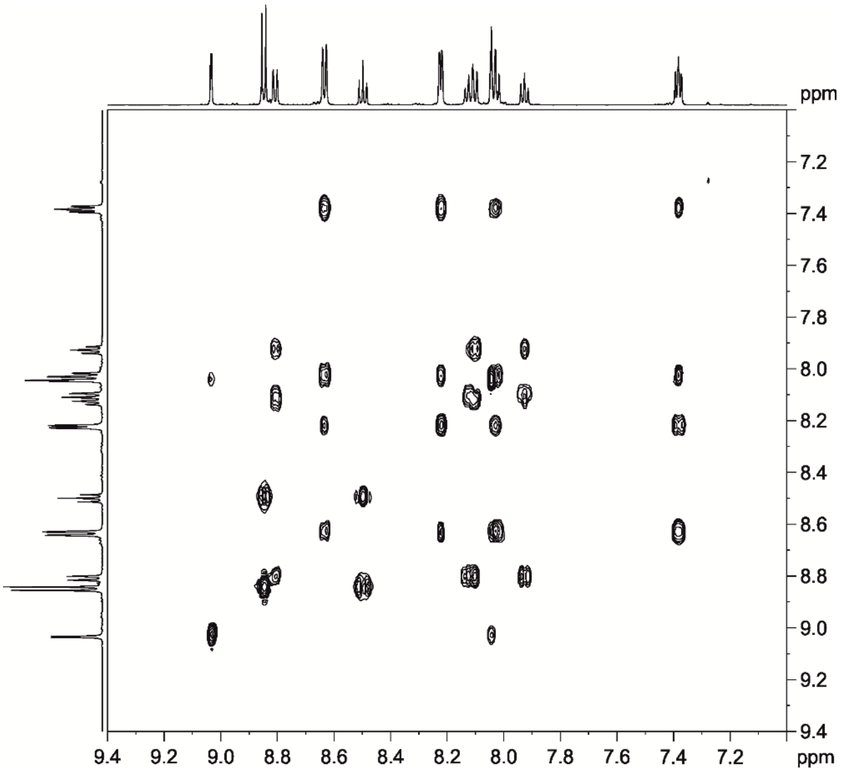
ppm
7.2
7.4
7.6
7.8
8.0
8.2
8.4
8.6
8.8
9.0
9.2
9.4
9.4
9.2
9.0
8.8
8.6
8.4
8.2
8.0
7.8
7.6
7.4
7.2
ppm

Figure S13. 1D and 2D NMR spectra of **4**$^{2+}$ (600 MHz, 298K, acetone-d$_6$): a) 1D ^{1}H, b) 1D ^{13}C{^{1}H}, c) 2D HSQC, d) 2D HMBC, e) 2D TOCSY, f) 2D ROESY.

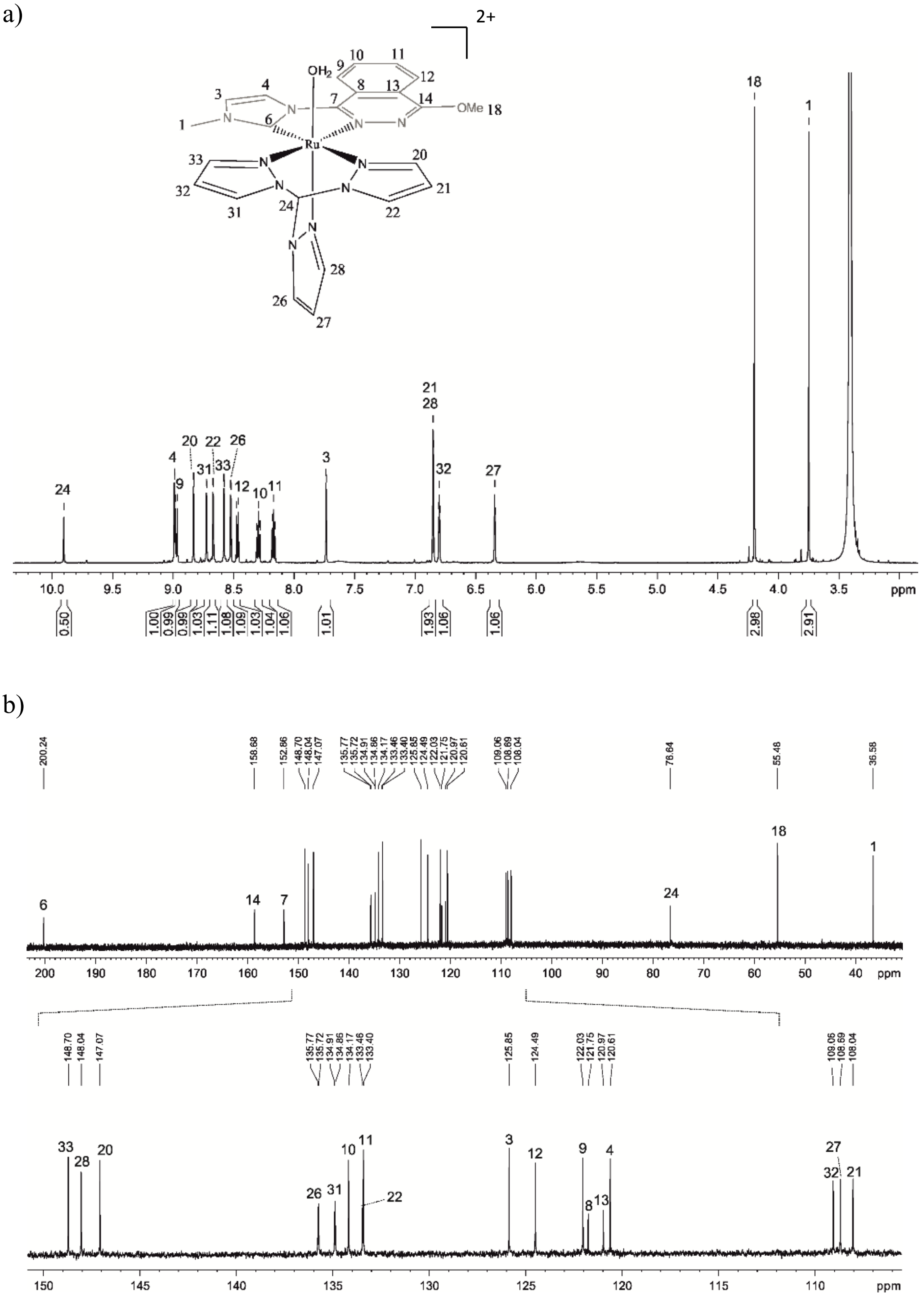

c)

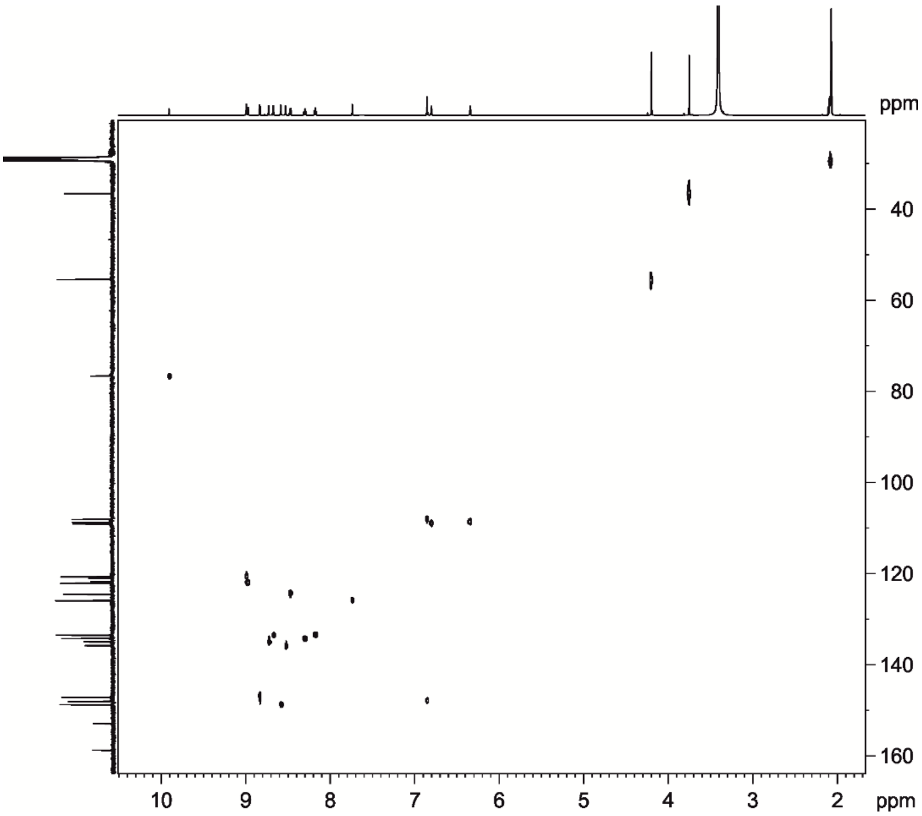
ppm
40
60
80
100
120
140
160
10
9
8
7
6
5
4
3
2
ppm

d)

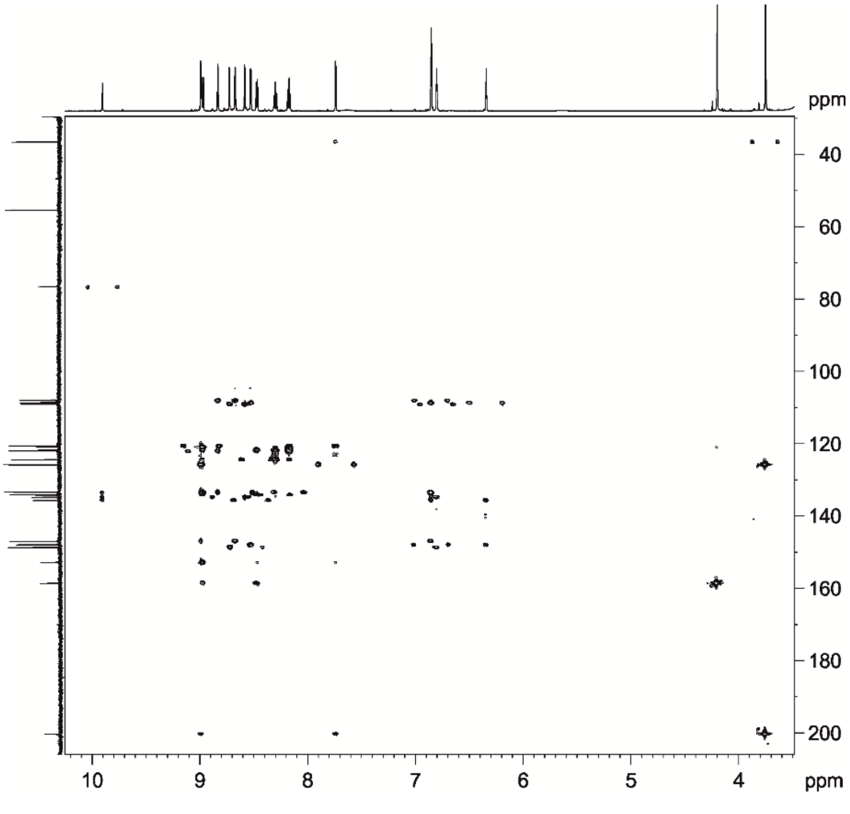
ppm
40
60
80
100
120
140
160
180
200
10
9
8
7
6
5
4
ppm

e)

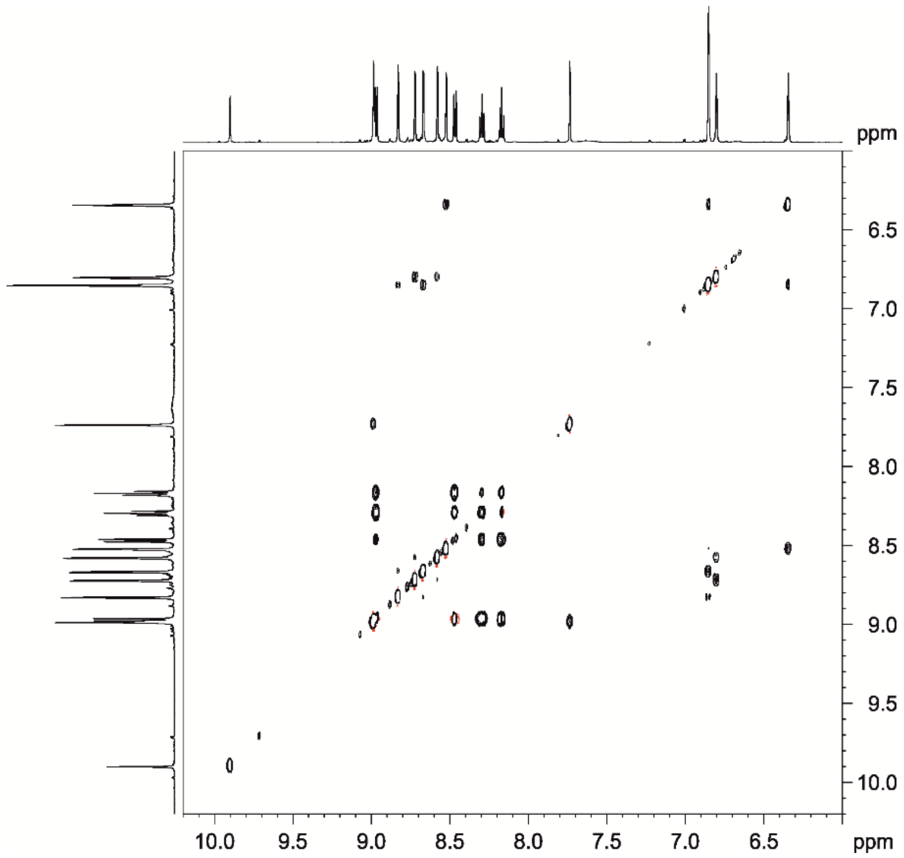
ppm
6.5
7.0
7.5
8.0
8.5
9.0
9.5
10.0
10.0
9.5
9.0
8.5
8.0
7.5
7.0
6.5
ppm

f)

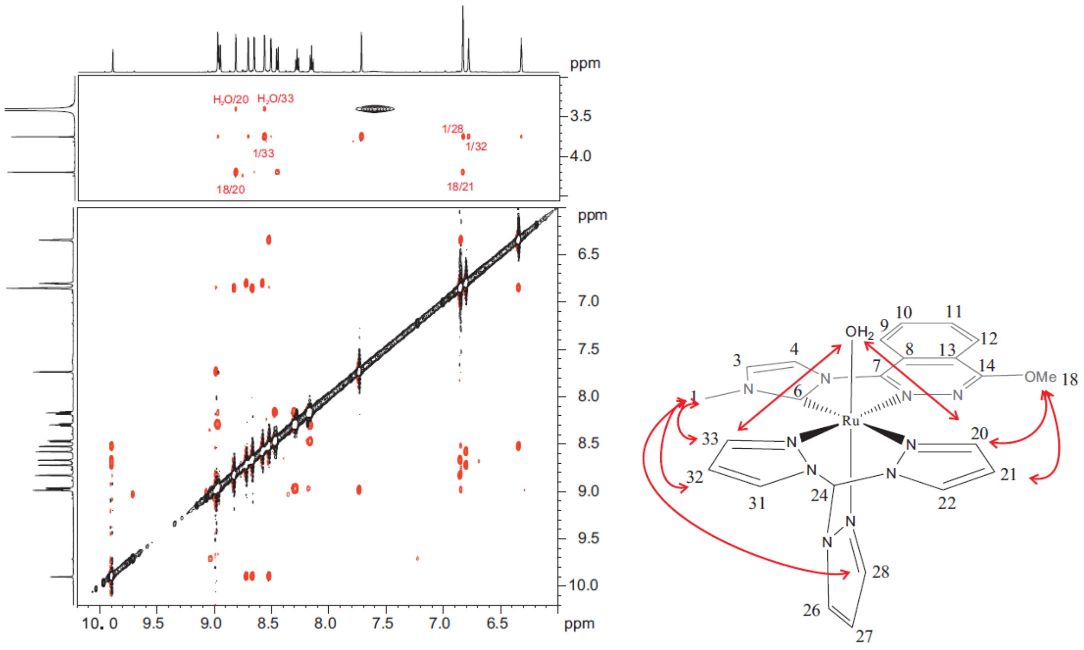
ppm
H$_2$O/20
H$_2$O/33
1/28
1/32
1/33
18/20
18/21
3.5
4.0
ppm
6.5
7.0
7.5
8.0
8.5
9.0
9.5
10.0
10.0
9.5
9.0
8.5
8.0
7.5
7.0
6.5
ppm
OH$_2$
Ru
OMe
N
1
3
4
6
7
8
9
10
11
12
13
14
18
20
21
22
24
26
27
28
31
32
33

Figure S14. 1D and 2D NMR spectra of **6**$^{2+}$ (600 MHz, 298K, acetone-d$_6$): a) 1D ^{1}H, b) 1D ^{1}H (aromatic region), c) 1D ^{13}C{^{1}H}, d) 2D HSQC, e) 2D HMBC, f) 2D TOCSY, g) 2D ROESY.

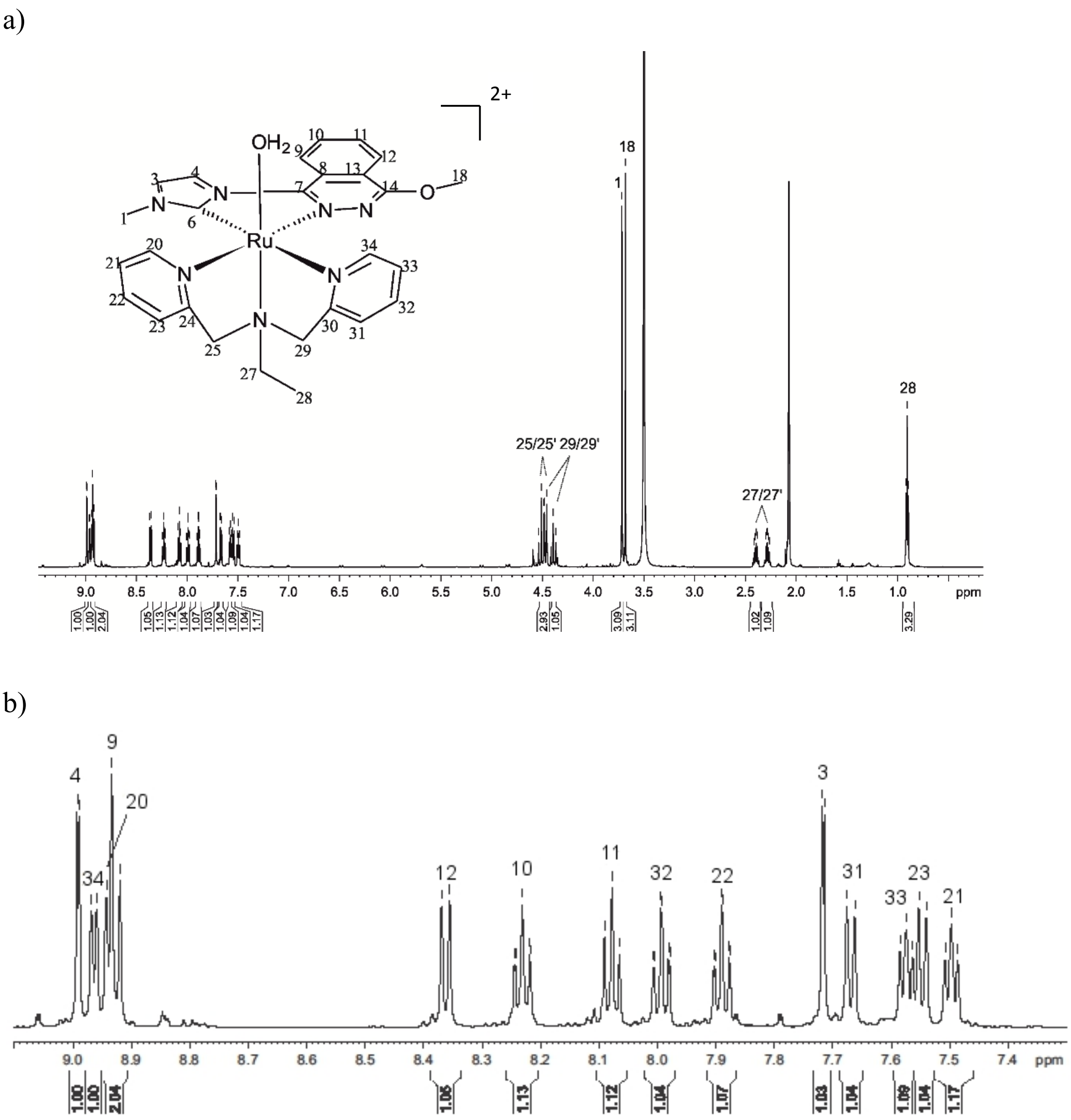

c)

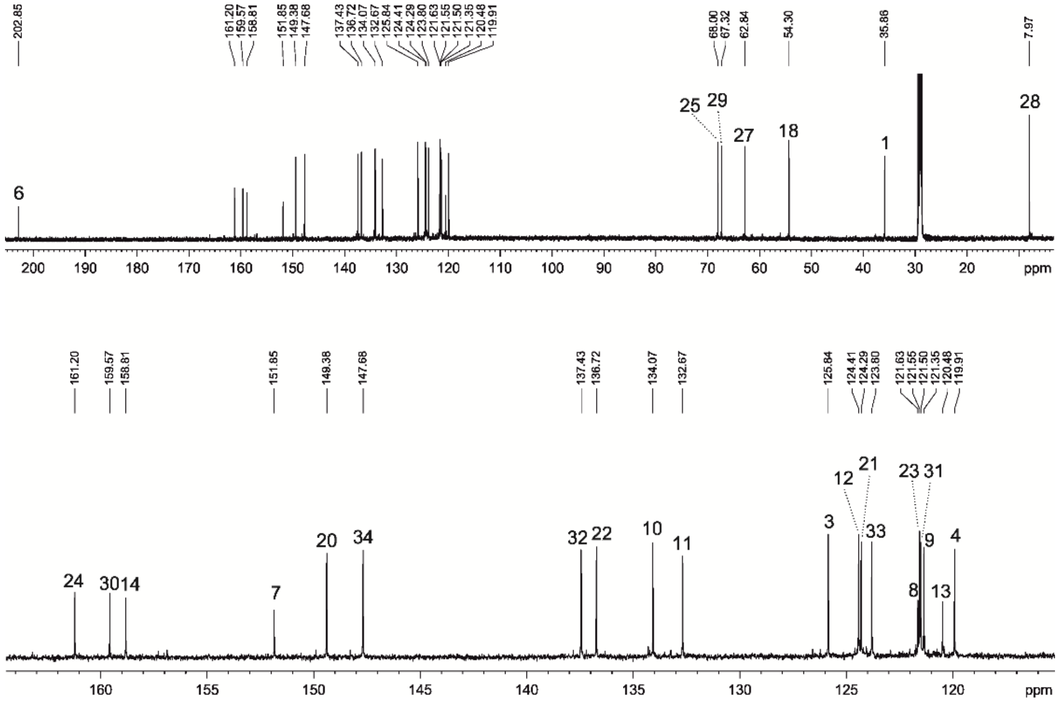
202.85
161.20
159.57
158.81
151.85
149.38
147.68
137.43
136.72
134.07
132.67
125.84
124.41
124.29
123.80
121.63
121.55
121.50
121.35
120.48
119.91
68.00
67.32
62.84
54.30
35.86
7.97
6
25
29
27
18
1
28
200
190
180
170
160
150
140
130
120
110
100
90
80
70
60
50
40
30
20
ppm
24
30
14
7
20
34
32
22
10
11
3
12
21
33
23
31
9
4
8
13
160
155
150
145
140
135
130
125
120
ppm

d)

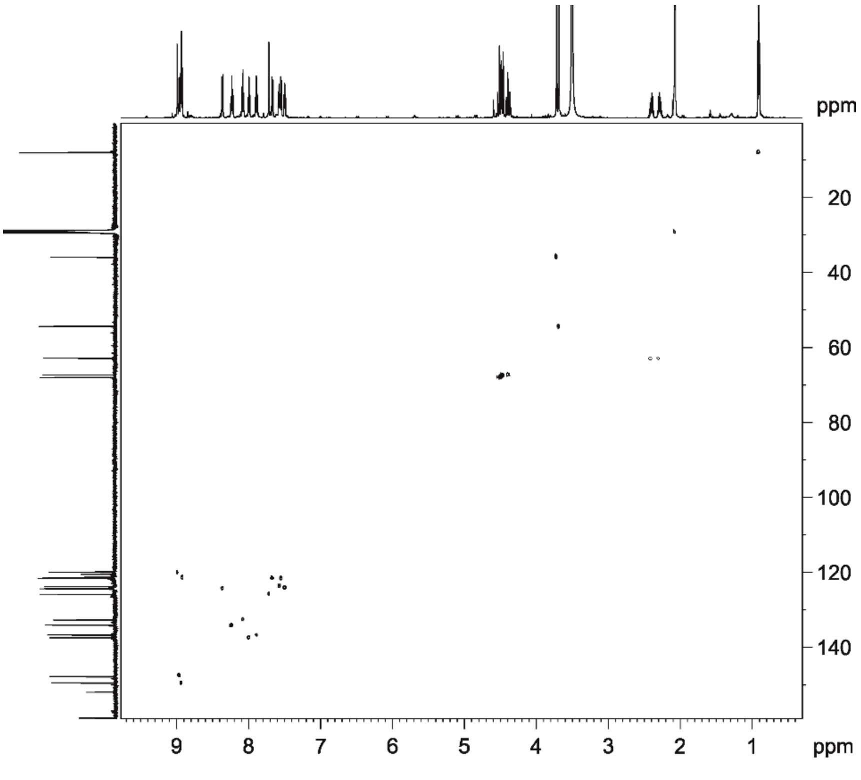
ppm
20
40
60
80
100
120
140
9
8
7
6
5
4
3
2
1
ppm

e)

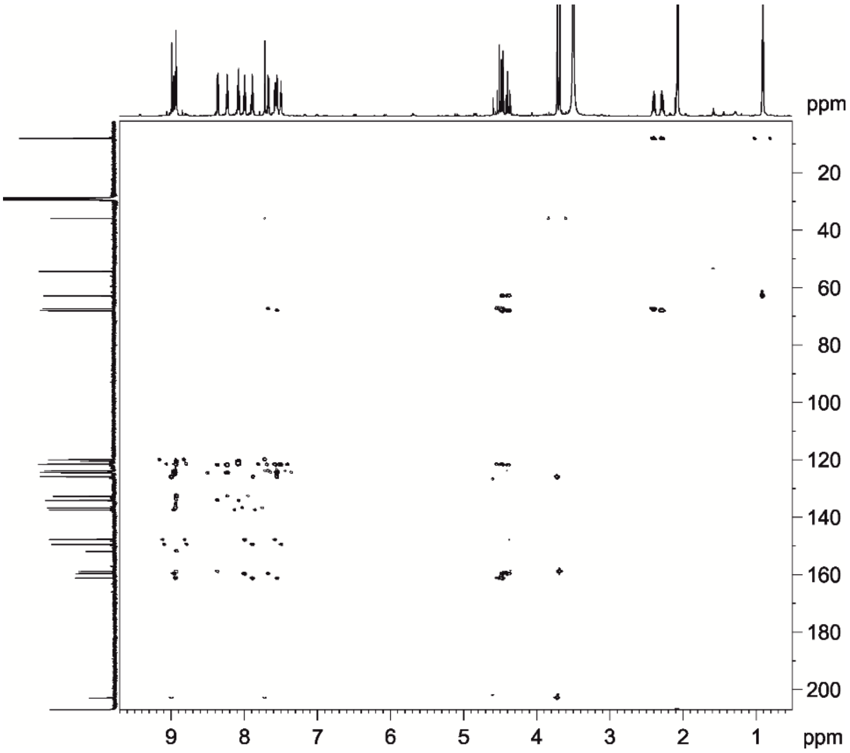
ppm
20
40
60
80
100
120
140
160
180
200
9
8
7
6
5
4
3
2
1
ppm

f)

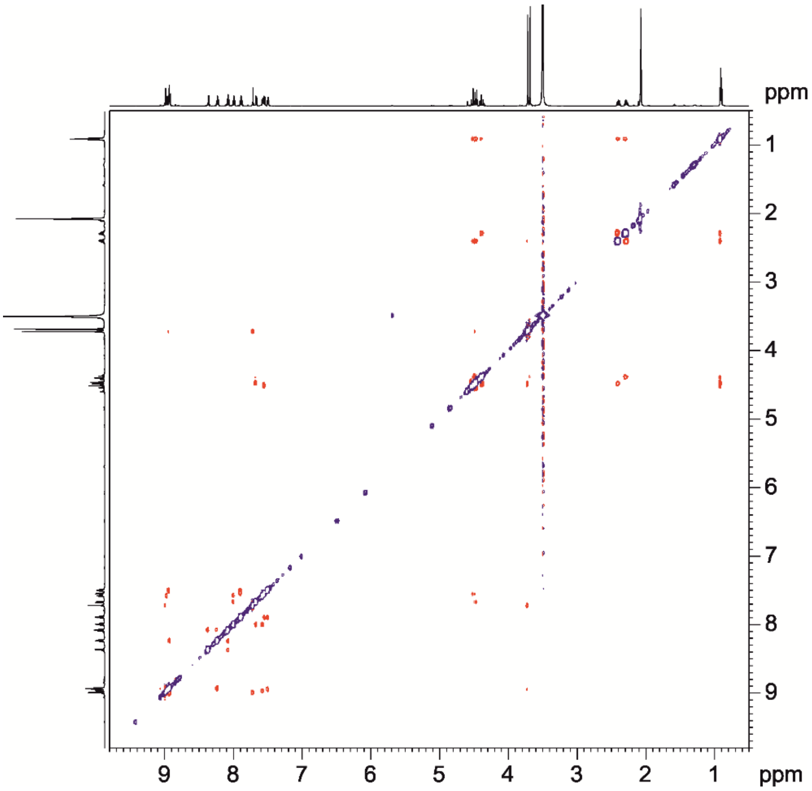
ppm
1
2
3
4
5
6
7
8
9
9
8
7
6
5
4
3
2
1
ppm

g)

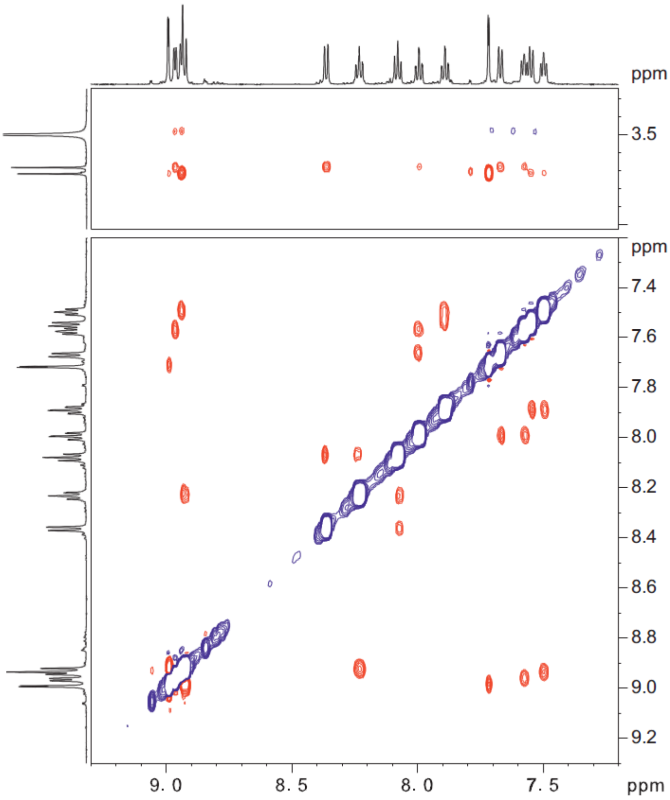

Figure S15. ESI-MS spectra of **2a**$^{2+}$ (a), **2b**$^{2+}$ (b), **4**$^{2+}$ (c) and **6**$^{2+}$ (d).

a)

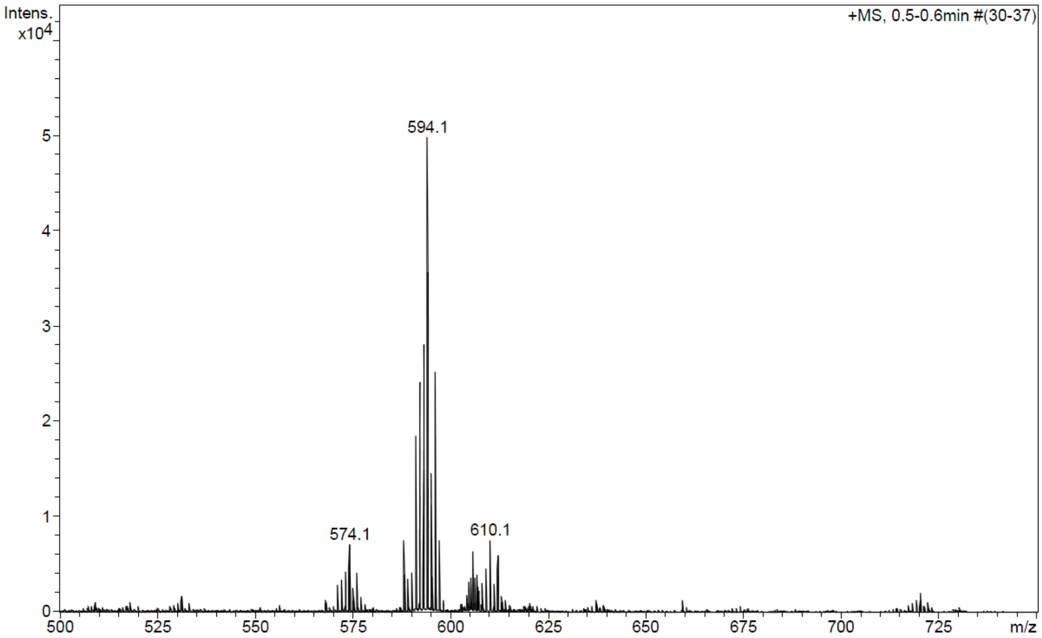

b)

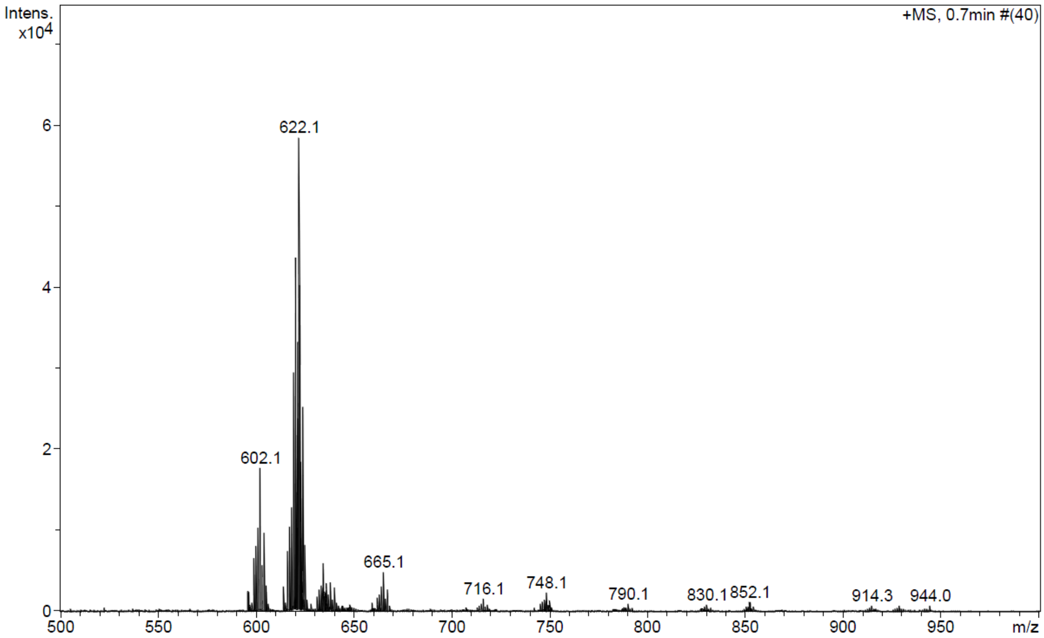

c)

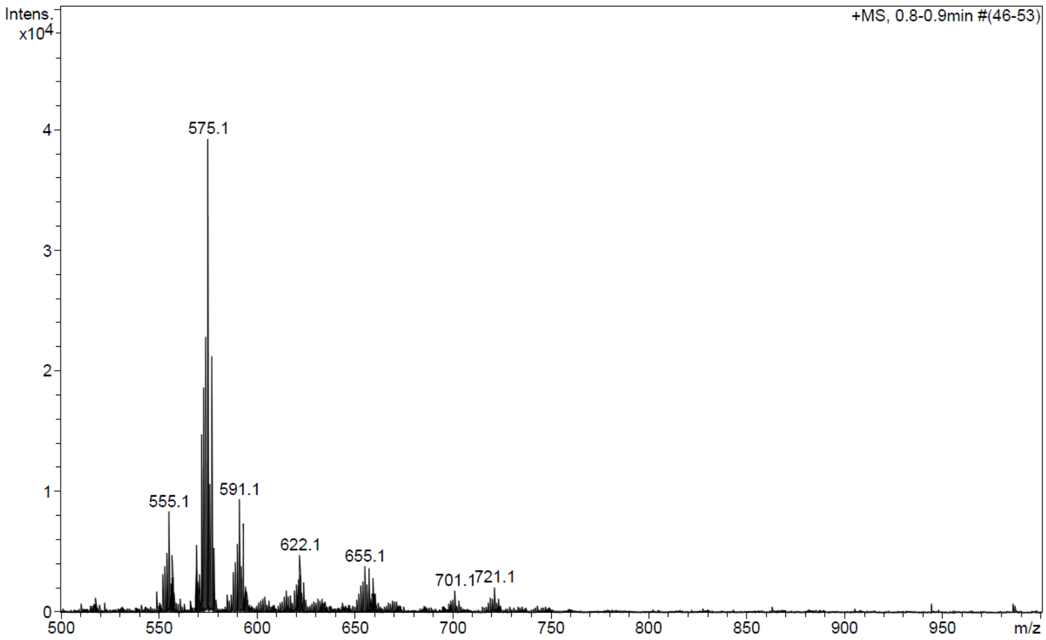
Intens.
x10^4
+MS, 0.8-0.9min #(46-53)
4
3
2
1
0
575.1
555.1
591.1
622.1
655.1
701.1
721.1
500
550
600
650
700
750
800
850
900
950
m/z

d)

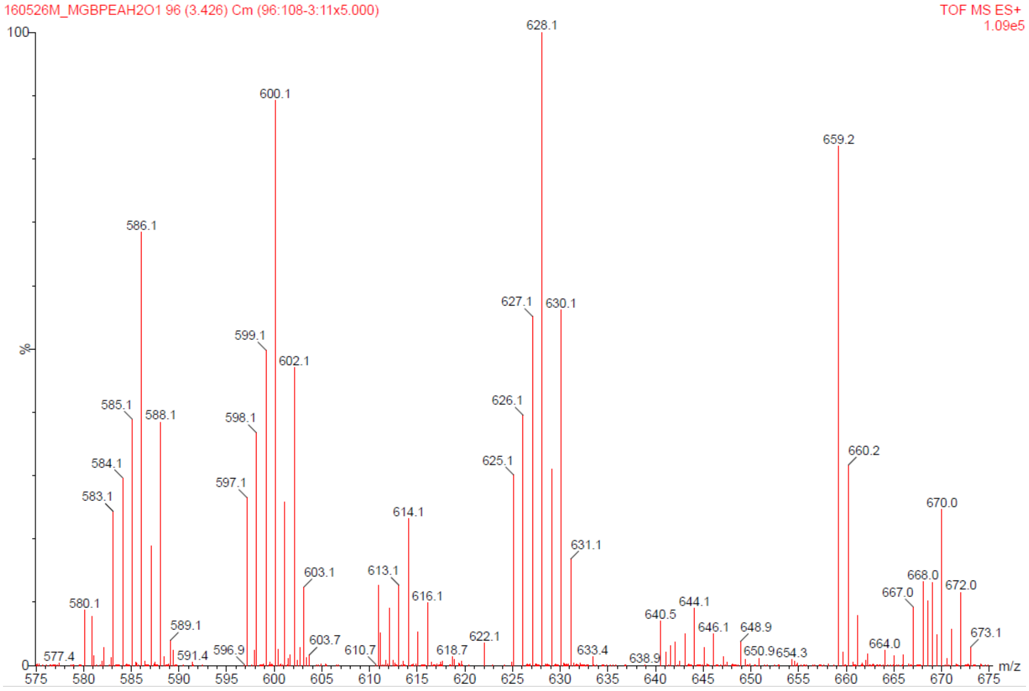
160526M_MGBPEAH2O1 96 (3.426) Cm (96:108-3:11x5.000)
TOF MS ES+
1.09e5
100
%
0
628.1
600.1
659.2
586.1
627.1
630.1
599.1
602.1
585.1
588.1
598.1
626.1
584.1
625.1
660.2
583.1
597.1
670.0
614.1
631.1
603.1
613.1
668.0
616.1
667.0
672.0
580.1
644.1
640.5
589.1
646.1
648.9
673.1
622.1
603.7
577.4
591.4
596.9
610.7
618.7
633.4
638.9
650.9
654.3
664.0
575
580
585
590
595
600
605
610
615
620
625
630
635
640
645
650
655
660
665
670
675
m/z

Figure S16. Cyclic Voltammetry of **1a**$^+$, **1b**$^+$, **3**$^+$ and **5**$^+$ in DCM (0.1 M TBAPF$_6$) at a 100 mV/s scan rate using a glassy carbon electrode as working electrode and a SCE as reference electrode.

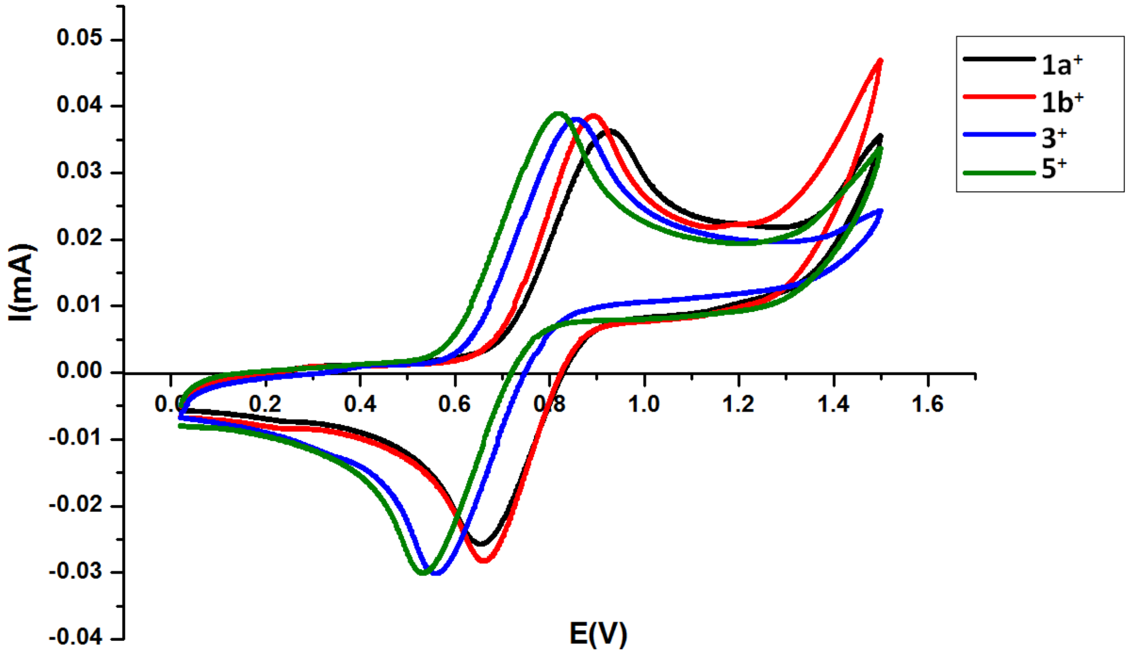

Figure S17. CV (a) and DPV (b) of **2a**$^{2+}$ in water at pH 1 (triflic acid buffer) and pH 8 (phosphate buffer) at a 100 mV/s scan rate. Glassy carbon has been used as working electrode and the potential has been measured *vs.* SCE.

a)

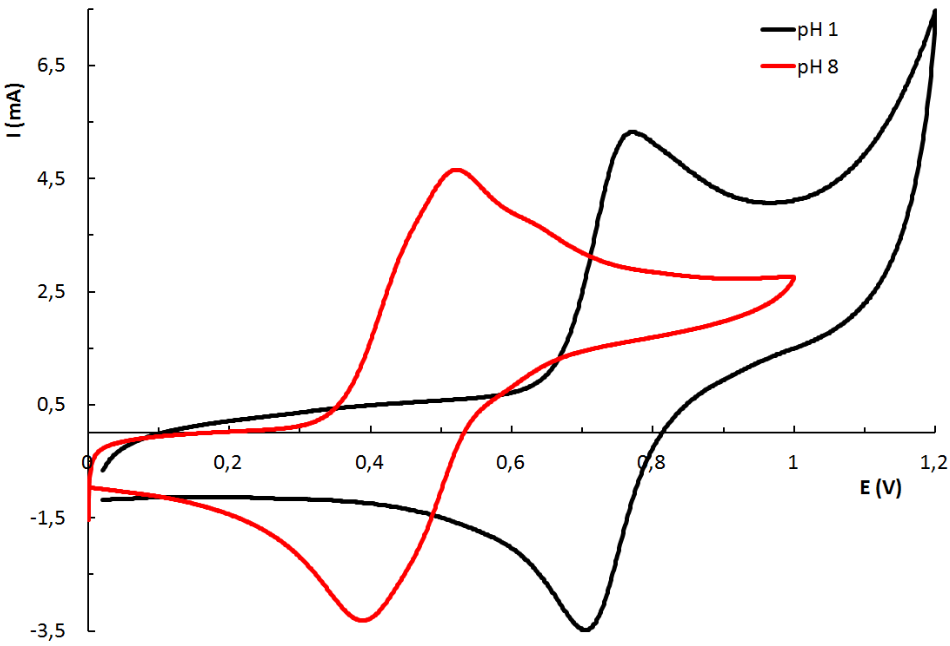

b)

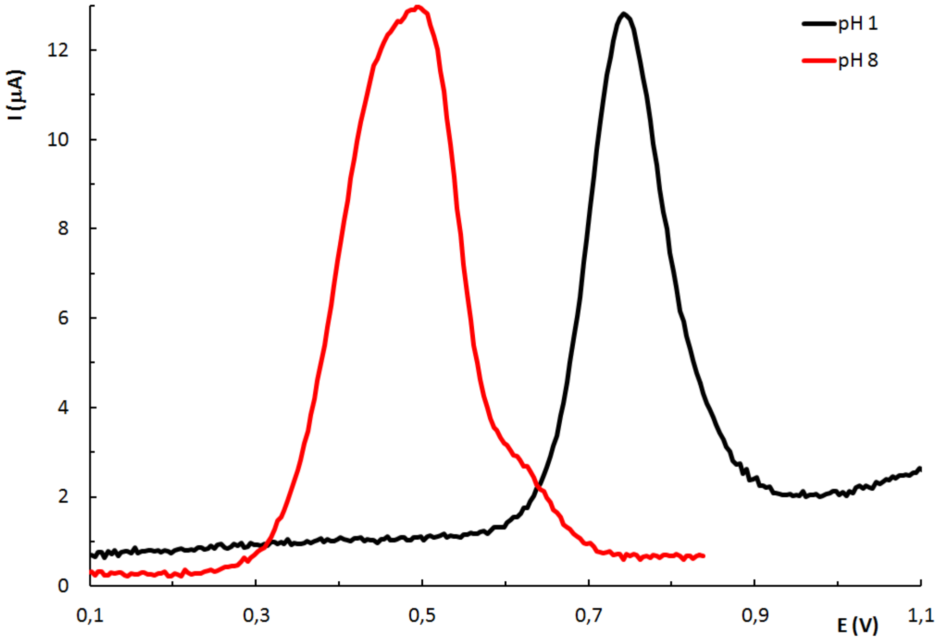

Figure S18. Bulk electrolysis experiments for **2a**$^{2+}$, **4**$^{2+}$ and **6**$^{2+}$. The electron transfer was calculated by $n_e = (I*t)/(n*F)$, where I is the current in mA, t is experimental time in s, n is mols of the complexes in mmol and F is Faraday constant.

a) Bulk electrolysis of **2a**$^{2+}$ in a pH 4.9 solution at an applied potential of 0.75 V vs. SCE.

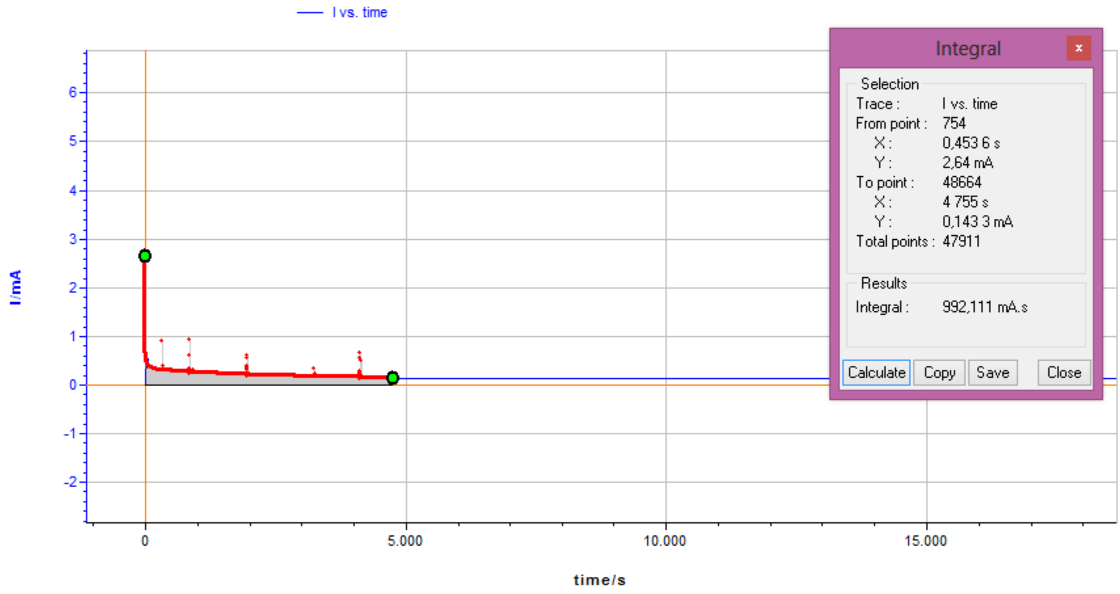

Selection
Trace : I vs. time
From point : 754
X : 0,453 6 s
Y : 2,64 mA
To point : 48664
X : 4 755 s
Y : 0,143 3 mA
Total points : 47911

Results
Integral : 992,111 mA.s

b) Bulk electrolysis of **4**$^{2+}$ in a pH 4.9 solution at an applied potential of 0.6 V vs SCE.

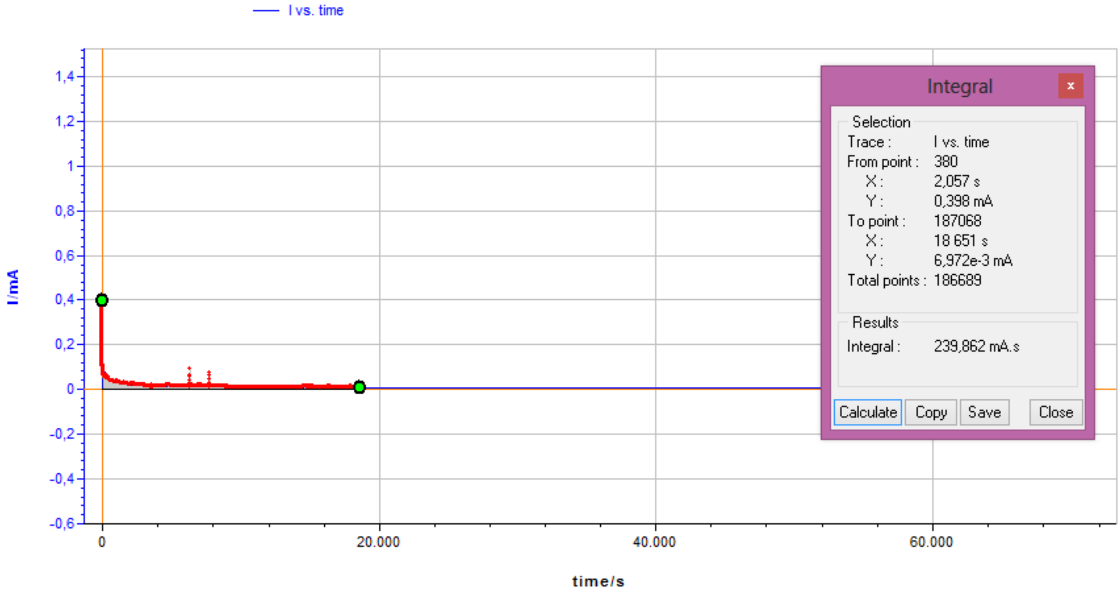

Selection
Trace : I vs. time
From point : 380
X : 2,057 s
Y : 0,398 mA
To point : 187068
X : 18 651 s
Y : 6,972e-3 mA
Total points : 186689

Results
Integral : 239,862 mA.s

c) Bulk electrolysis of **6**$^{2+}$ in a pH 4.9 solution at an applied potential of 0.57 V vs. SCE.

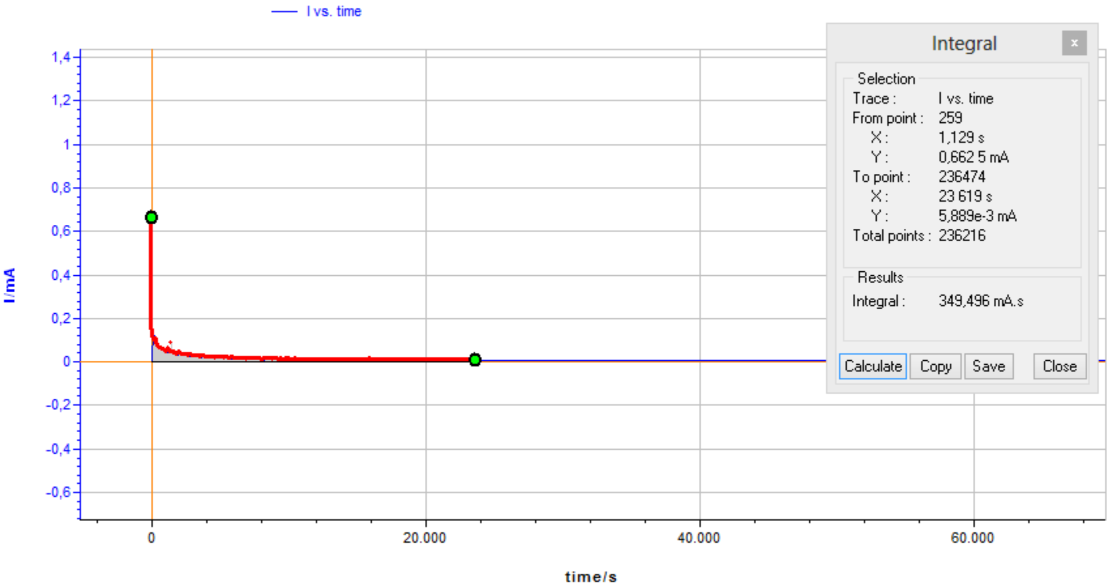

Selection
Trace : I vs. time
From point : 259
X : 1,129 s
Y : 0,662 5 mA
To point : 236474
X : 23 619 s
Y : 5,889e-3 mA
Total points : 236216

Results
Integral : 349,496 mA.s

d) Bulk electrolysis of **6**$^{2+}$ in a pH 4.9 solution at an applied potential of 0.75 V vs. SCE.

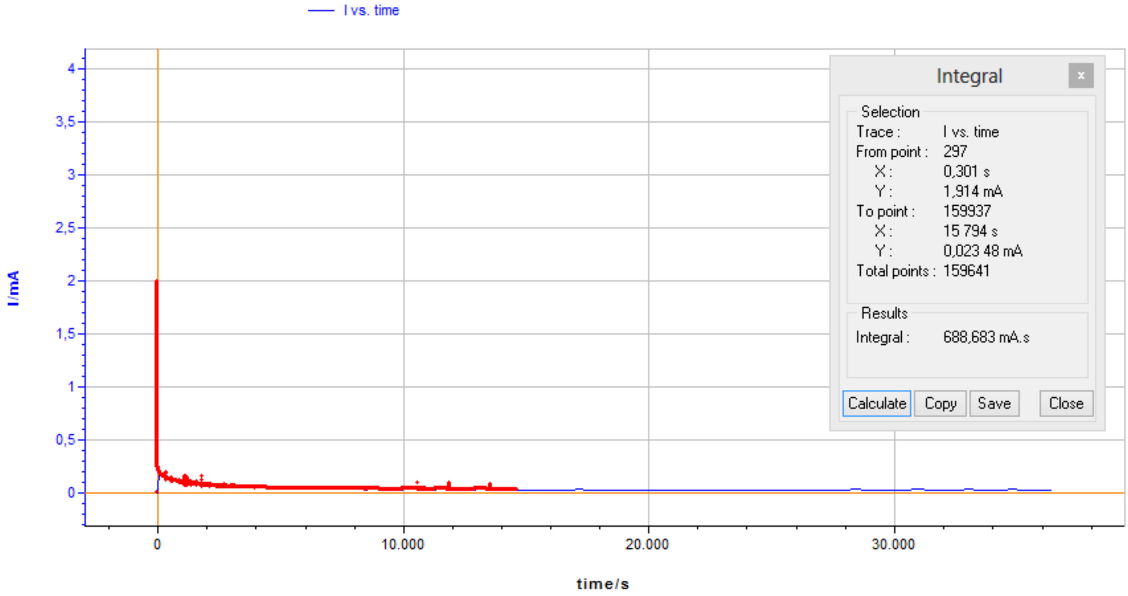

Selection
Trace : I vs. time
From point : 297
X : 0,301 s
Y : 1,914 mA
To point : 159937
X : 15 794 s
Y : 0,023 48 mA
Total points : 159641

Results
Integral : 688,683 mA.s

Figure S19. CV (a) and DPV (b) of **2b**$^{2+}$ in water at pH 1 (triflic acid buffer) and pH 8 (phosphate buffer) at a 100 mV/s scan rate. Glassy carbon has been used as working electrode and the potential has been measured *vs.* SCE.

a)

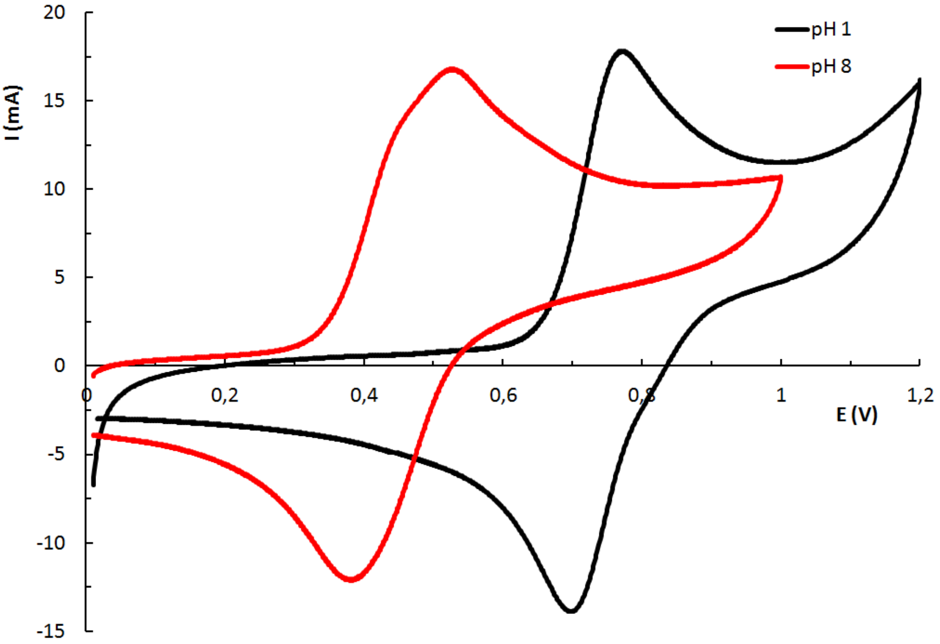

b)

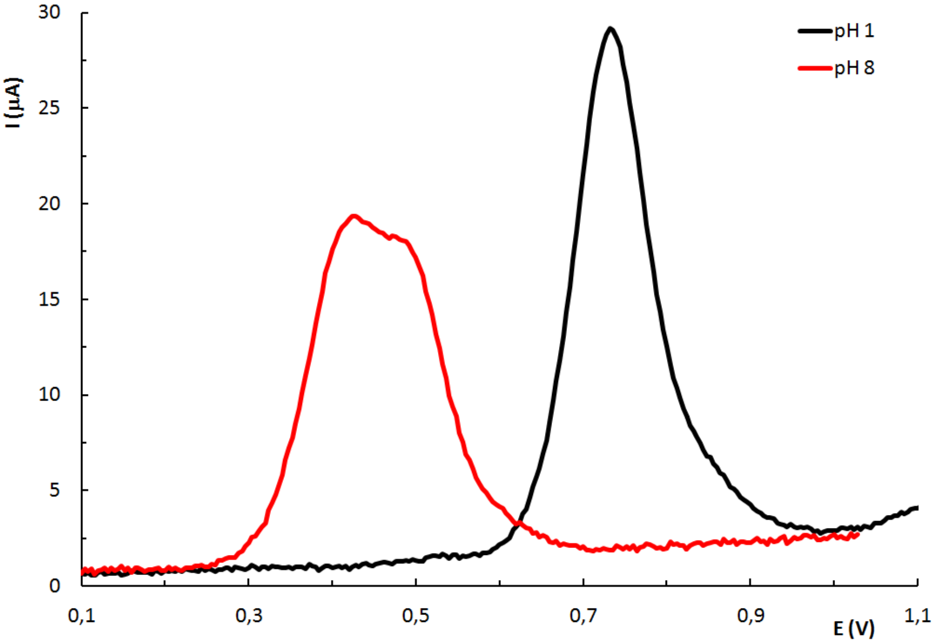

Figure S20. Plot of $E_{1/2}$ *vs.* pH (Pourbaix diagram) for complex **2b**$^{2+}$. The pH/potential regions of stability for the various oxidation states and their dominant proton compositions are indicated by using abbreviations such as Ru^{II}-OH_2, for example, for $[Ru^{II}(iPr\text{-}\mathbf{L2})(OH_2)(trpy)]^{2+}$. The vertical lines in the various E/pH regions show the pKa values.

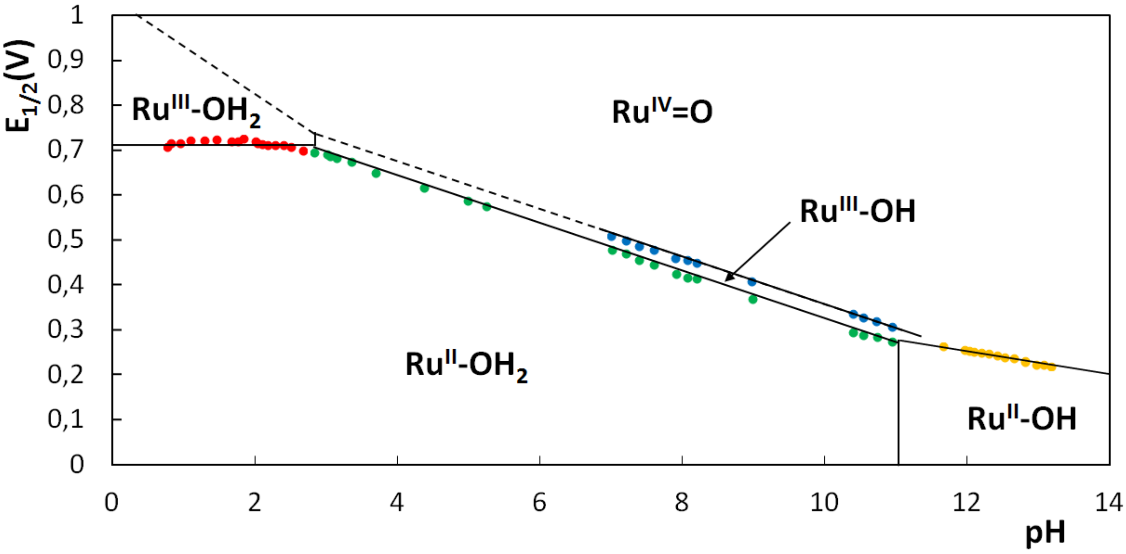

Figure S21. CV (a) and DPV (b) of $\mathbf{4}^{2+}$ in water at pH 1 (triflic acid buffer) and pH 8 (phosphate buffer) at a 100 mV/s scan rate. Glassy carbon has been used as working electrode and the potential has been measured *vs.* SCE.

a)

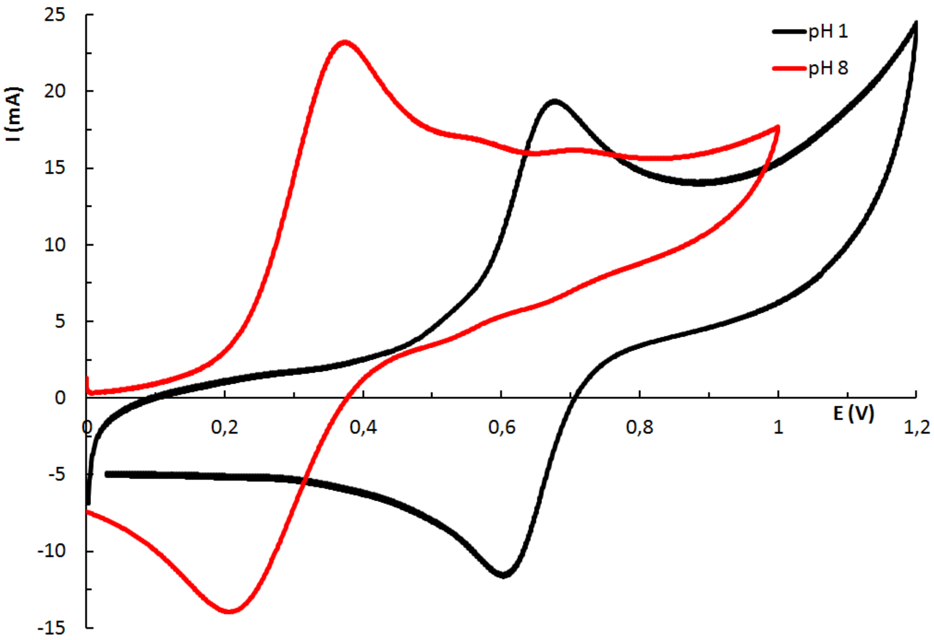

b)

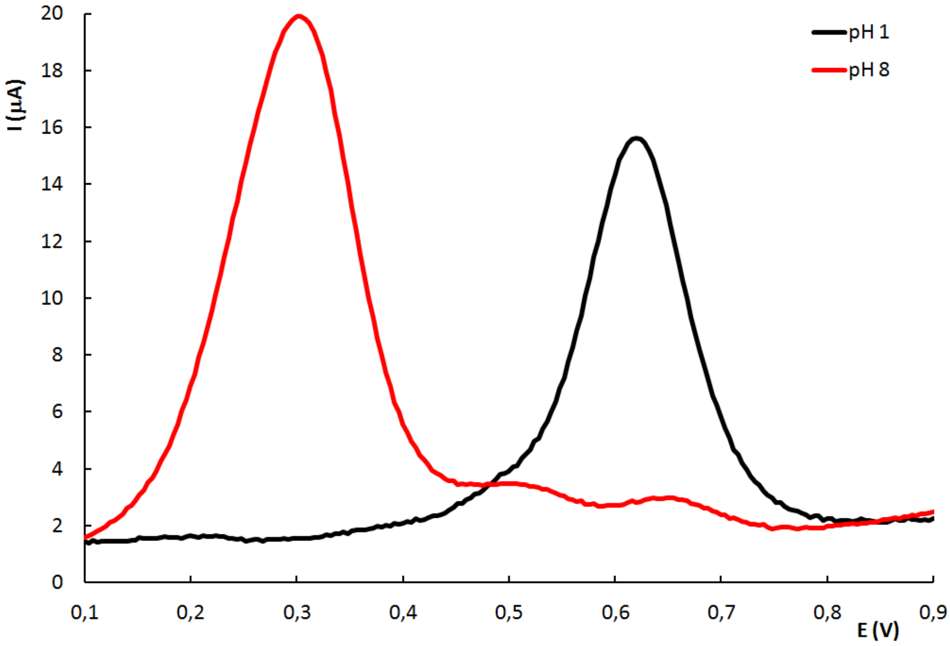

Figure S22. CV (a) and DPV (b) of **6**$^{2+}$ in water at pH 1 (triflic acid buffer) and pH 8 (phosphate buffer) at a 100 mV/s scan rate. Glassy carbon has been used as working electrode and the potential has been measured *vs.* SCE.

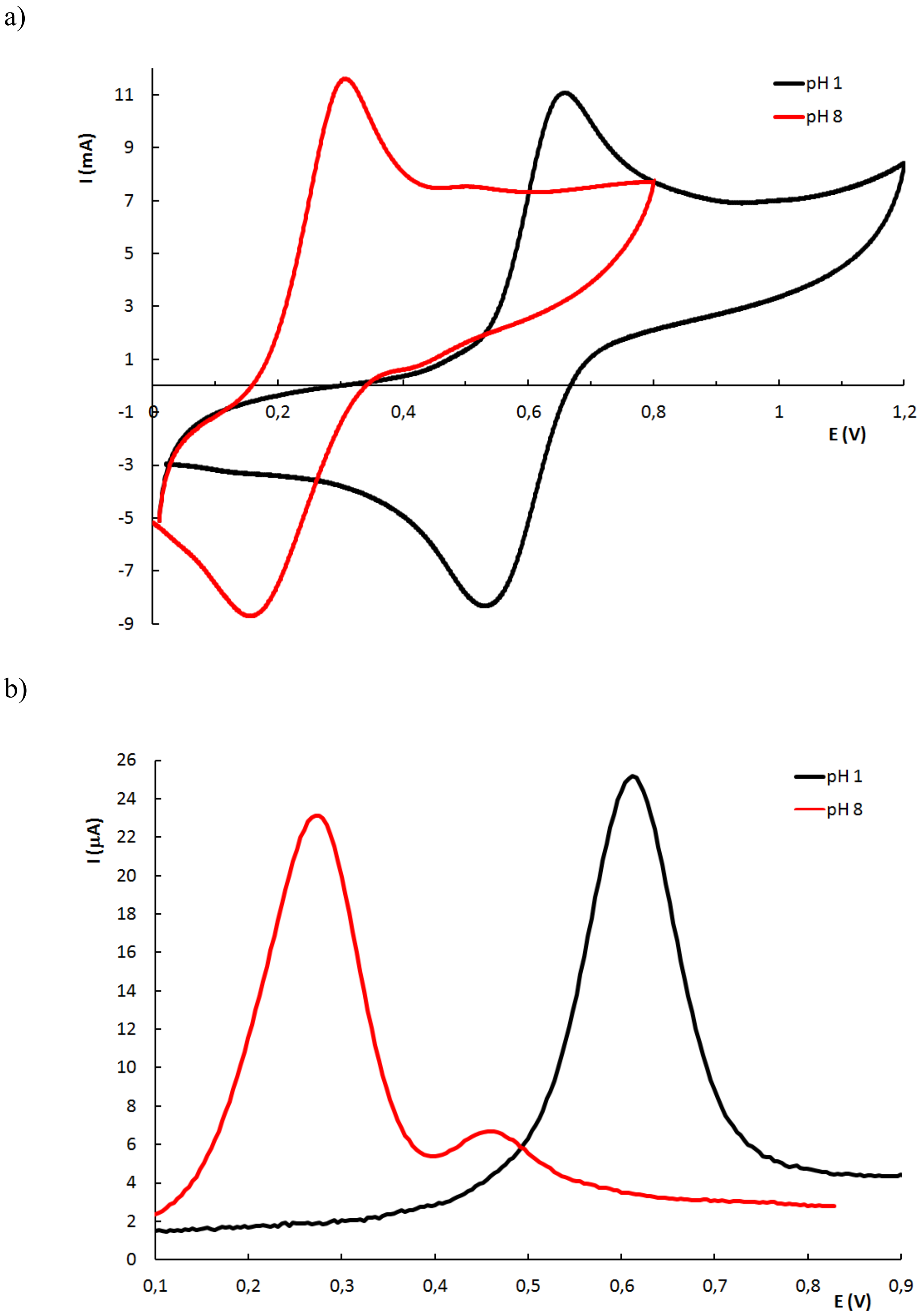

Figure S23. UV-vis spectra for **1a**$^{+}$/**2a**$^{2+}$, **1b**$^{+}$/**2b**$^{2+}$, **3**$^{+}$/**4**$^{2+}$ and **5**$^{+}$/**6**$^{2+}$ solutions at 50 μM concentration in MeOH.

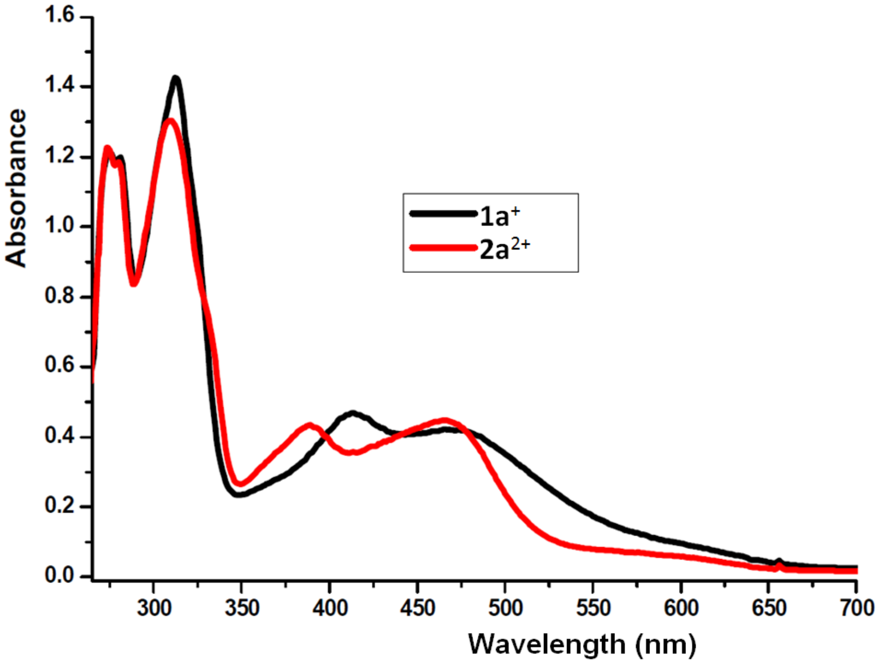

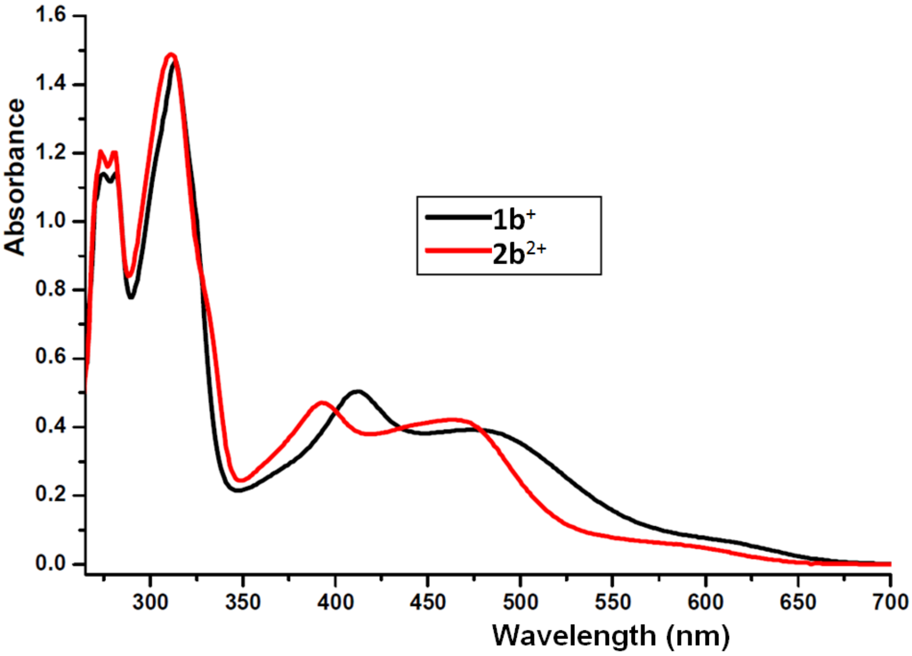

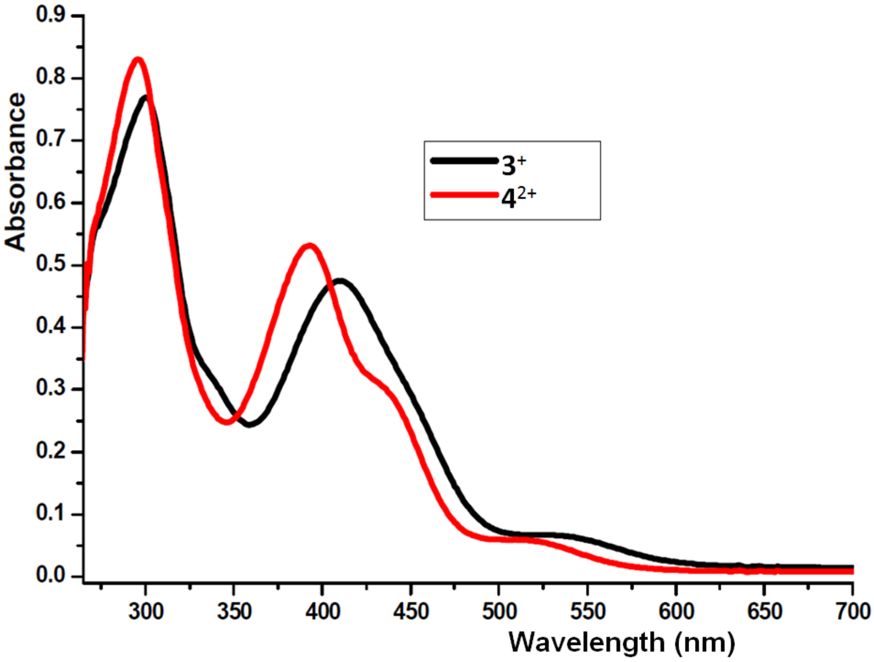
0.9
0.8
0.7
0.6
0.5
0.4
0.3
0.2
0.1
0.0
Absorbance
300
350
400
450
500
550
600
650
700
Wavelength (nm)
3^+
4^{2+}

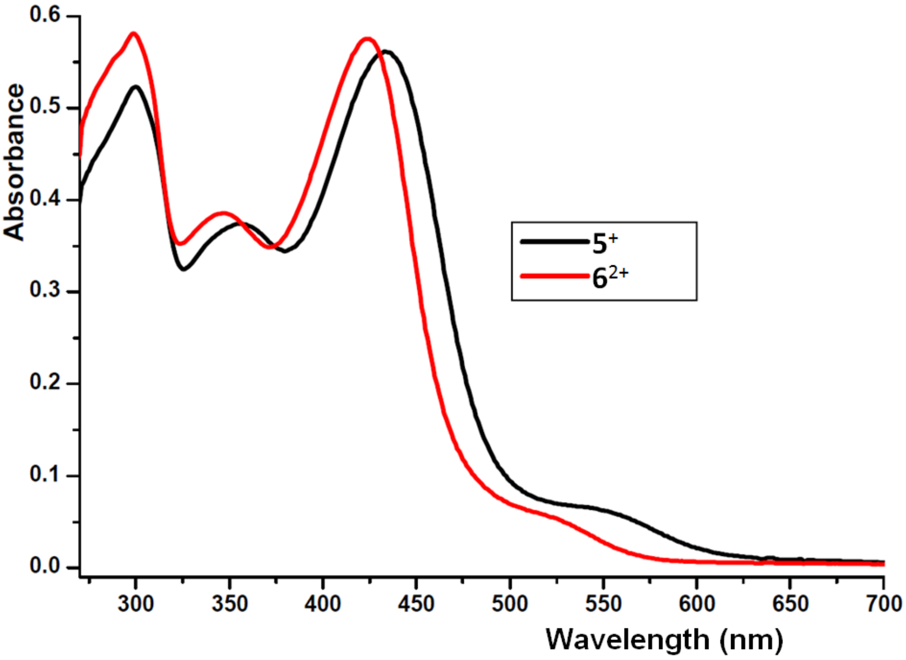
0.6
0.5
0.4
0.3
0.2
0.1
0.0
Absorbance
300
350
400
450
500
550
600
650
700
Wavelength (nm)
5^+
6^{2+}

Figure S24. DPVs for the determination of E^0_{PQ} of **2a**$^{2+}$ (a), **4**$^{2+}$ (b) and **6**$^{2+}$ (c) in aqueous triflic acid 0.1 M (pH 1.0). DPV registered at pulses height (P_H) 50 mV, pulses width (P_W) 50 ms, sampling width (S_W) 16 ms and pulse period 500 ms.

a)

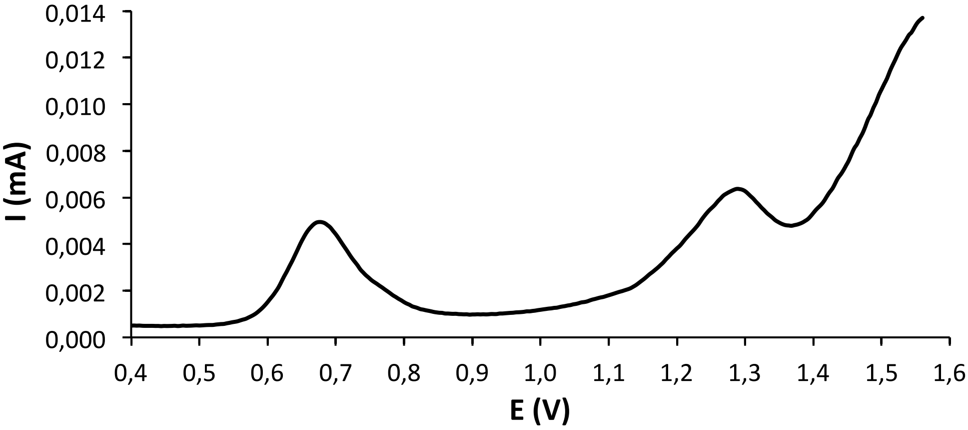

b)

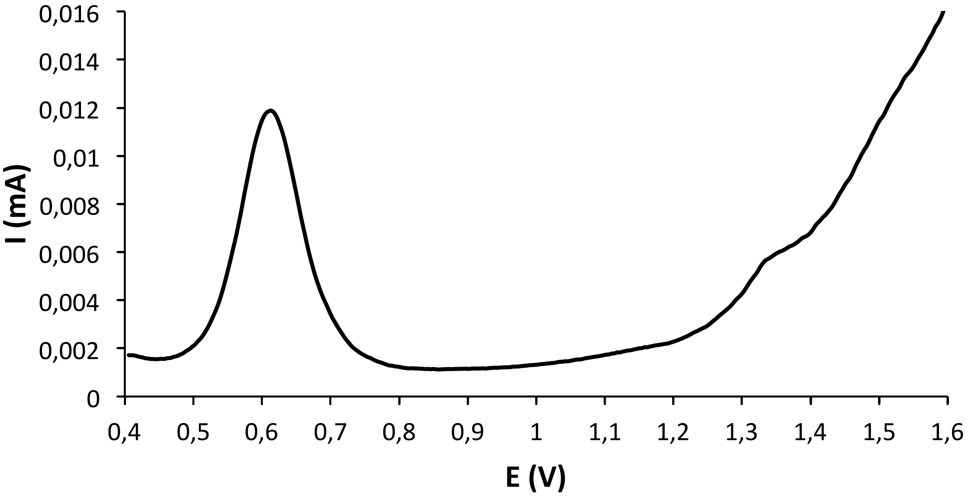

c)

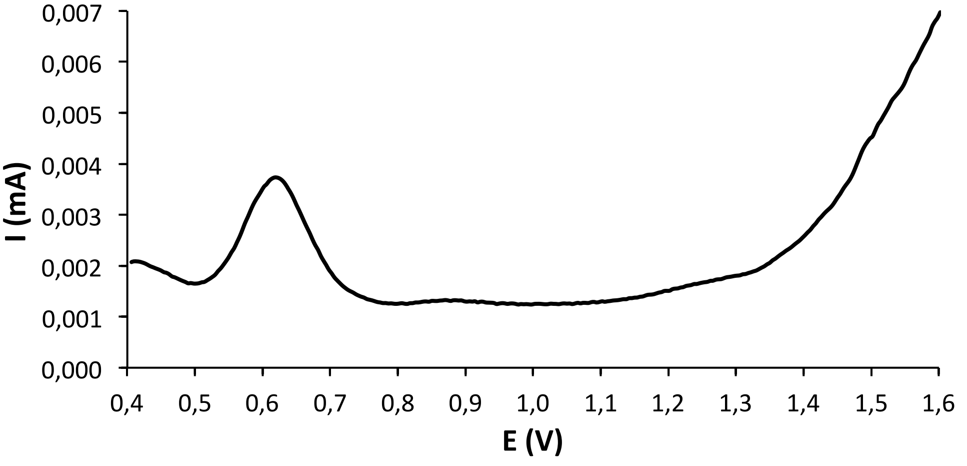

Figure S25. Background corrected CVs of a 0.64 mM solution of $\mathbf{2a}^{2+}$ (a) and a 0.68 mM solution of $\mathbf{6}^{2+}$ (b) in aqueous triflic acid 0.1 M (pH 1.0) at 100 mV/s scan rate. Foot-of-the-wave analysis of $\mathbf{2a}^{2+}$ (c) and $\mathbf{6}^{2+}$ (d). Insets: plot of the different k_{obs} values extracted from the foot-of-the-wave analysis at each concentration. The blue line represents the trend of the k_{obs} values.

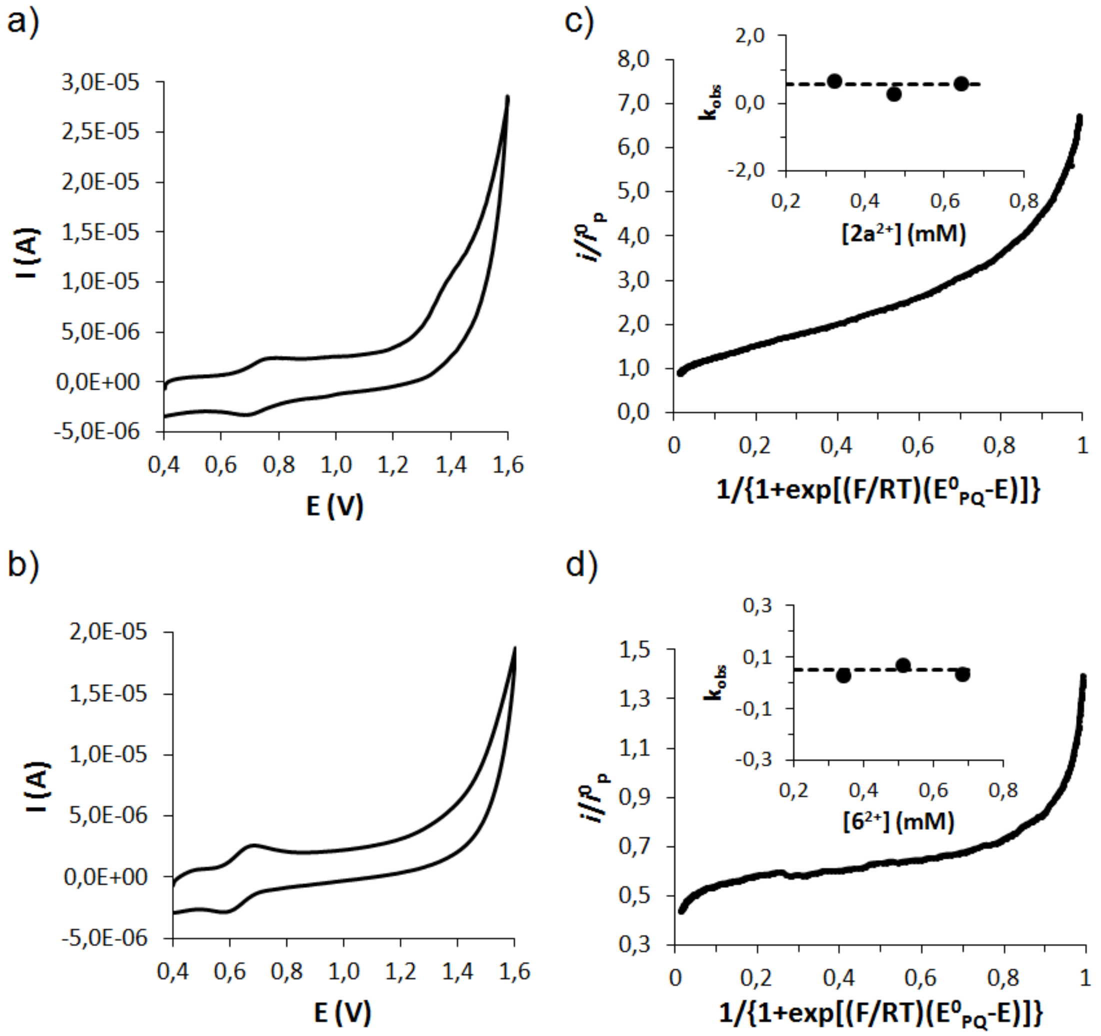

Figure S26. Manometric profile of evolved gases for complexes **2a**$^{2+}$, **2b**$^{2+}$, **4**$^{2+}$ and **6**$^{2+}$ in a pH 1 aqueous solution using $(NH_4)_2Ce^{IV}(NO_3)_6$ as sacrificial oxidant. Cat:Ce(IV) = 1:100.

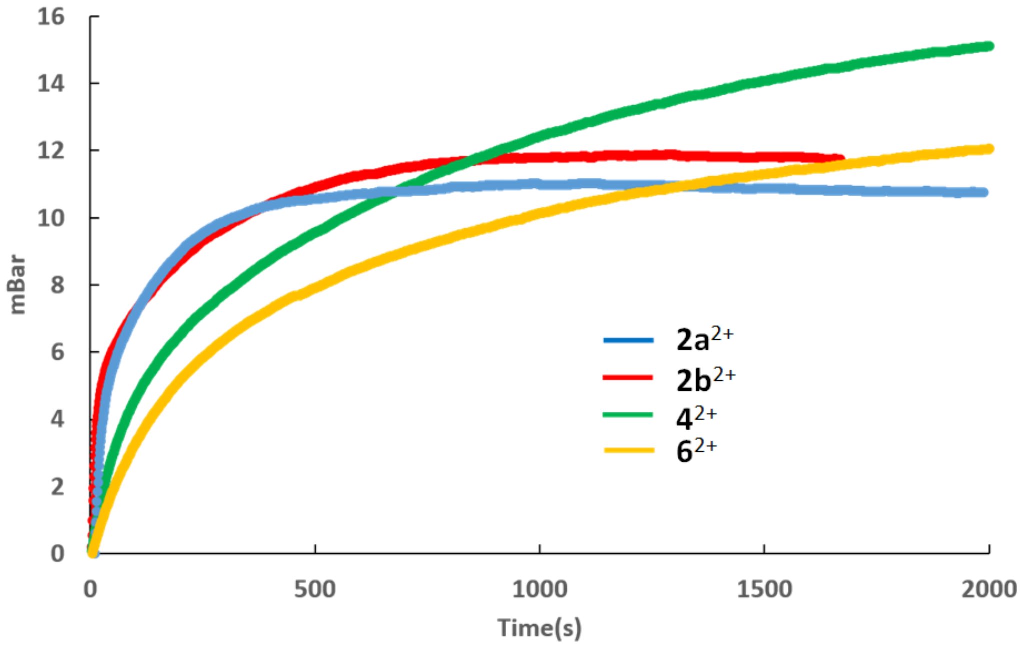

Figure S27. Mass Spectrometry profile of the generated gases upon oxidative treatment of **2a**$^{2+}$ (a), **2b**$^{2+}$ (b), **4**$^{2+}$ (c) and **6**$^{2+}$ (d) with $(NH_4)_2Ce^{IV}(NO_3)_6$ at pH 1. Cat:Ce(IV) = 1:100.

a)

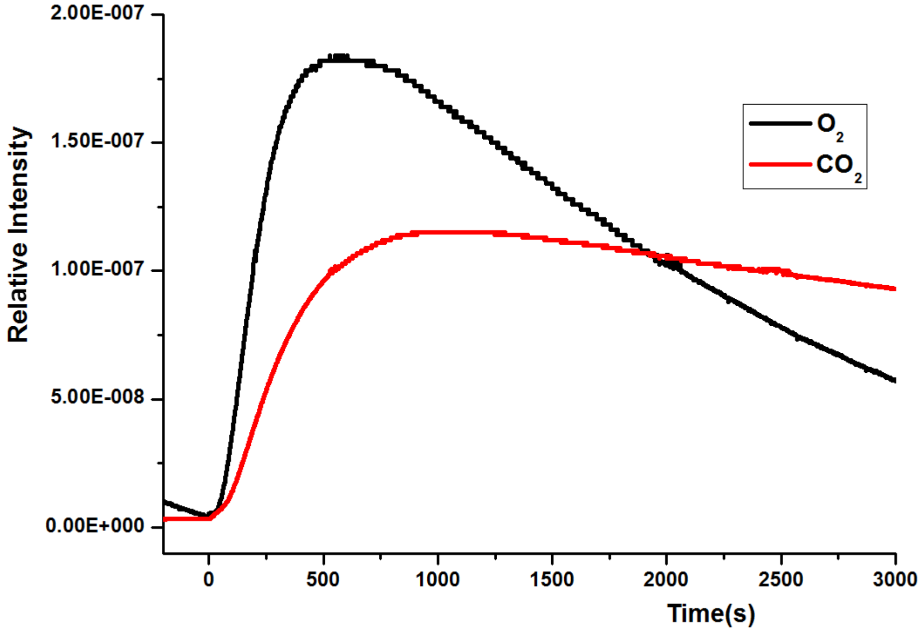

b)

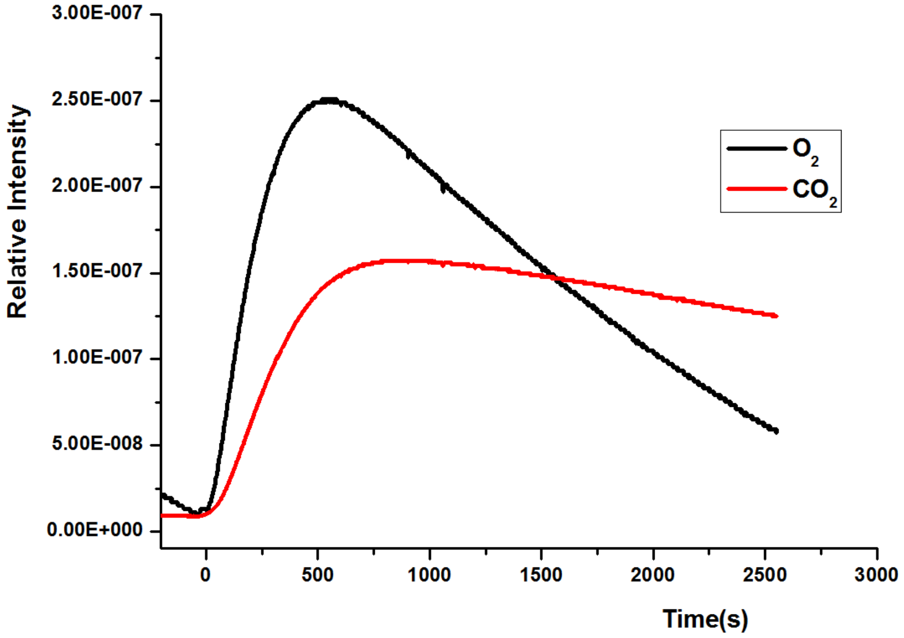

c)

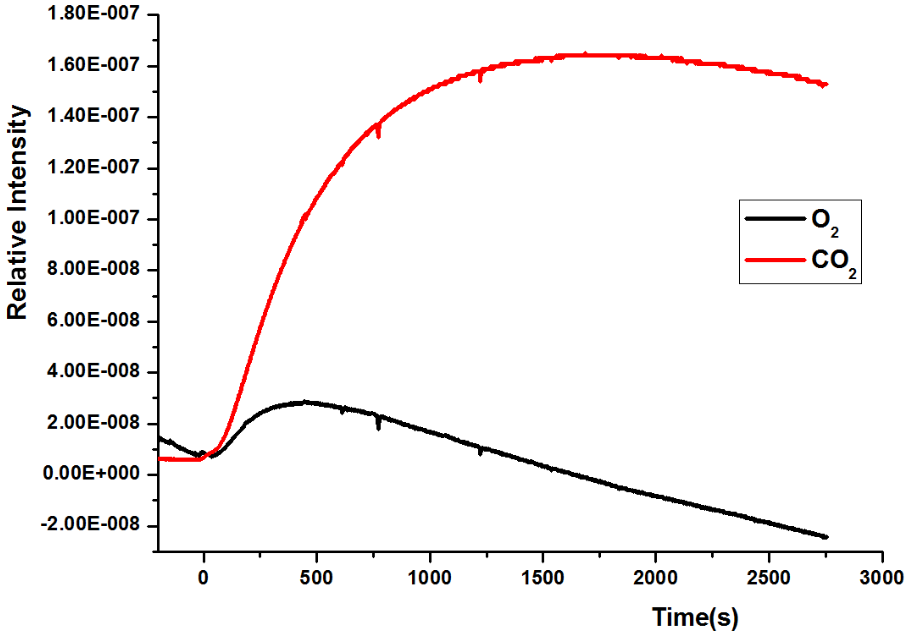
1.80E-007
1.60E-007
1.40E-007
1.20E-007
1.00E-007
8.00E-008
6.00E-008
4.00E-008
2.00E-008
0.00E+000
-2.00E-008
Relative Intensity
0
500
1000
1500
2000
2500
3000
Time(s)
O_2
CO_2

d)

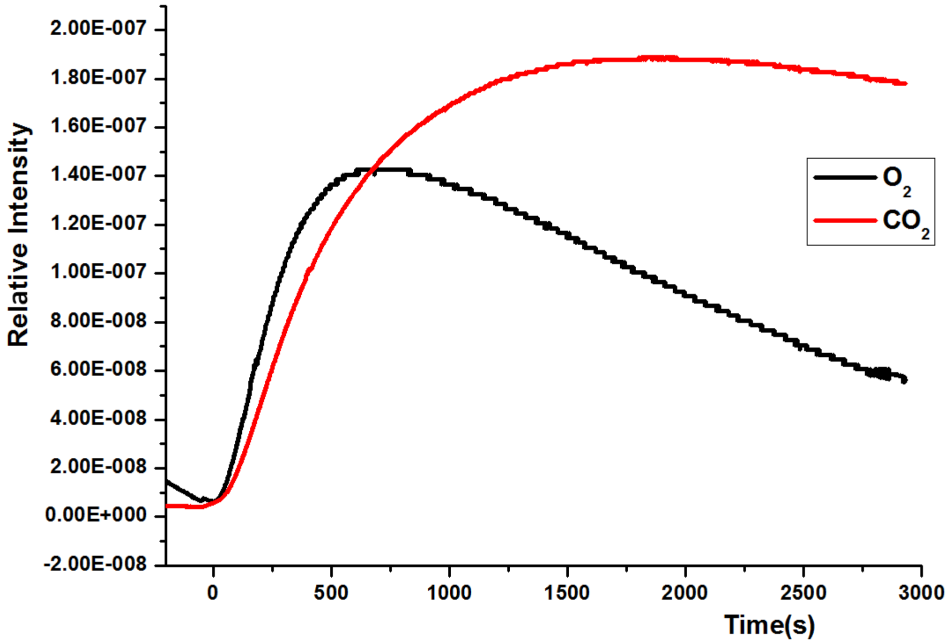
2.00E-007
1.80E-007
1.60E-007
1.40E-007
1.20E-007
1.00E-007
8.00E-008
6.00E-008
4.00E-008
2.00E-008
0.00E+000
-2.00E-008
Relative Intensity
0
500
1000
1500
2000
2500
3000
Time(s)
O_2
CO_2

Figure S28. Oxygen evolution profile of at pH 1 for the four aqua complexes employing $(NH_4)_2Ce^{IV}(NO_3)_6$ as sacrificial oxidant. Cat:Ce(IV) = 1:100.

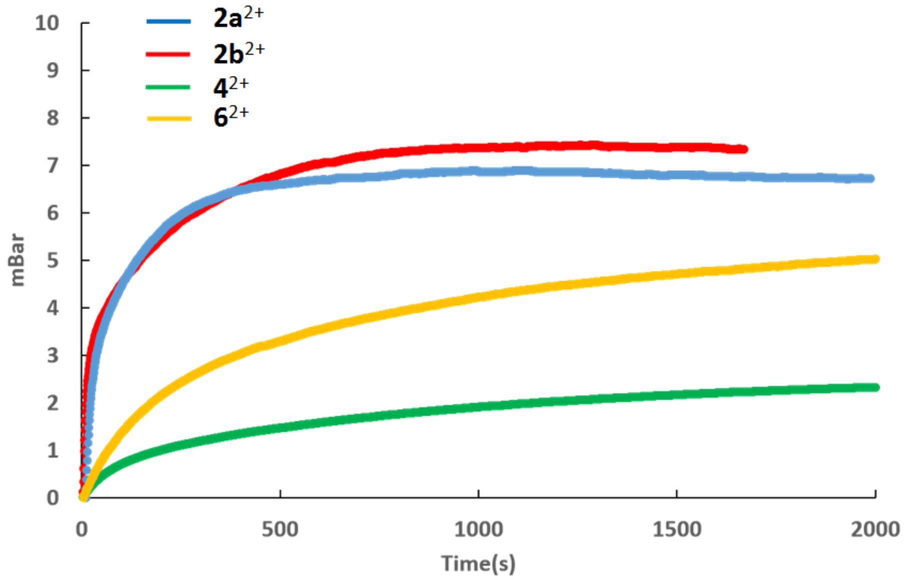

Scheme S1. Proposed nucleophilic attack of the solvent leading to the breakage of H_2**L1**$^{2+}$ during the synthesis of the chloro complexes **1a**$^+$, **1b**$^+$, **3**$^+$ and **5**$^+$.

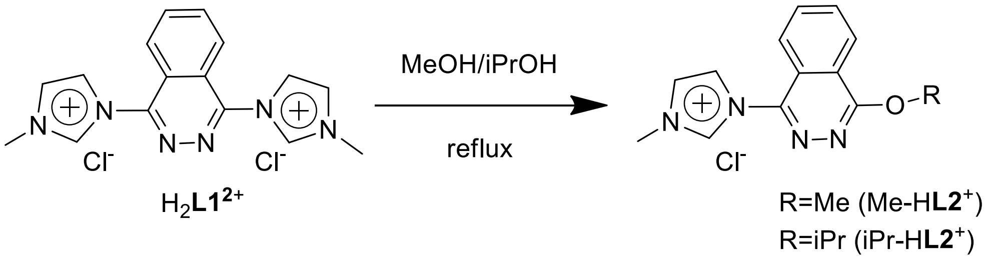

Scheme S2. Proposed reactions taking place during the catalytic epoxidation of alkenes by the four aqua complexes.

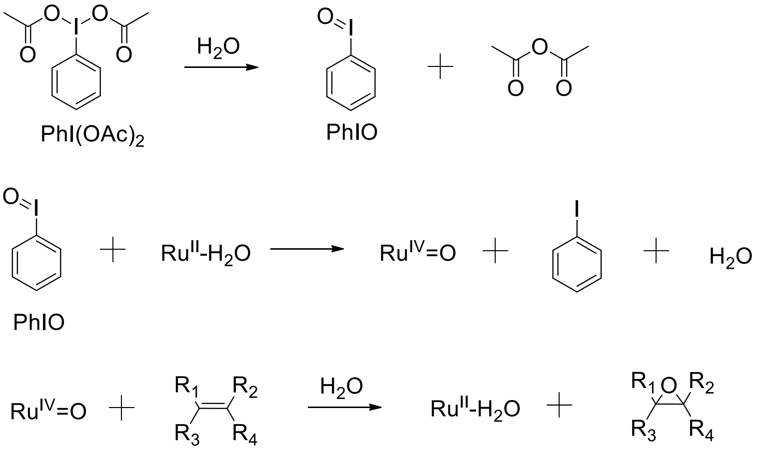

Scheme S3. Possible mechanisms occurring during the catalytic epoxidation of alkenes by the four aqua complexes.

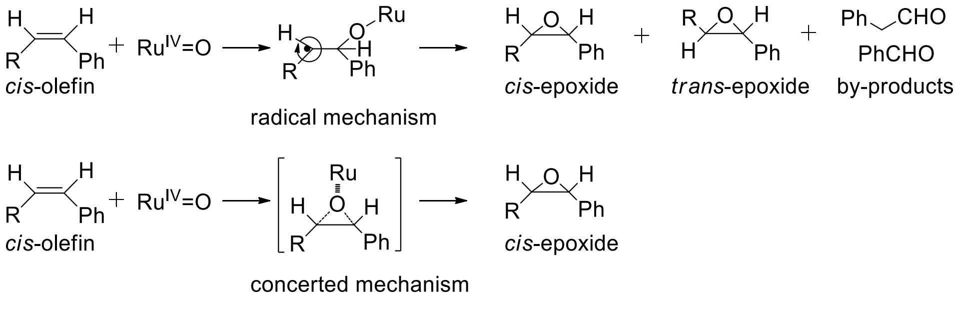

Table S1. Crystallographic data for H_2**L1**$(PF_6)_2$.

Empirical formula	C16 H16 F12 N6 P2
Formula weight	582.29
Temperature	298(2) K
Wavelength	0.71073 Å
Crystal system	Monoclinic
Space group	P2(1)/c
Unit cell dimensions	a = 17.64(6) Å α = 90°
	b = 12.59(4) Å β= 101.23(7) °
	c = 18.67(6) Å γ = 90°
Volume	4065(22) Å^3
Z	8
Calculated density	1.903 Mg/m^3
Absorption coefficient	0.344 mm^{-1}
F(000)	2336
Crystal size	0.30 × 0.30 × 0.25 mm^3
Theta range for data collection	1.96 to 29.66°
Limiting indices	-24<=h<=24, -17<=k<=17, -25<=l<=25
Reflections collected / unique	68116 / 11227 [R(int) = 0.2510]
Completeness to theta = 29.66	97.7 %
Absorption correction	Empirical
Max. and min. transmission	1.0 and 0.388546
Refinement method	Full-matrix least-squares on F^2
Data / restraints / parameters	11227 / 0 / 649
Goodness-of-fit on F2	1.016
Final R indices [I>2sigma(I)]	R1 = 0.0940, wR2 = 0.2072
R indices (all data)	R1 = 0.3097, wR2 = 0.2912
Largest diff. peak and hole	0.592 and -0.387 e.Å^{-3}

Table S2. Selected interatomic distances (Å) and angles (°) for the cationic part of **5**(PF_6).

Bond distances			
Ru-C6	1.962(4)	Ru-N1	2.130(4)
Ru-N4	2.014(4)	Ru-N3	2.139(4)
Ru-N2	2.066(4)	Ru-Cl	2.4088(12)
Angles			
C6-Ru-N4	77.44(16)	N4-Ru-Cl	88.04(11)
C6-Ru-N2	101.35(16)	N2-Ru-N1	81.68(15)
C6-Ru-N1	98.55(16)	N2-Ru-N3	83.78(13)
C6-Ru-N3	174.78(16)	N2-Ru-Cl	94.92(12)
C6-Ru-Cl	87.60(13)	N1-Ru-N3	81.15(14)
N4-Ru-N2	176.80(15)	N1-Ru-Cl	171.63(10)
N4-Ru-N1	95.54(14)	N3-Ru-Cl	90.90(11)
N4-Ru-N3	97.38(14)		

Table S3. Crystallographic data for **5**(PF_6).

Identification code	mo_HJCAt4_0m
Empirical formula	C27 H29 Cl F6 N7 O P Ru
Formula weight	749.06
Temperature	100(2) K
Wavelength	0.71073 Å
Crystal system	Triclinic
Space group	P-1
Unit cell dimensions	a = 7.8526(10)Å α= 75.184(4)°.
	b = 12.5701(14)Å β= 79.085(4)°.
	c = 16.1322(19)Å γ= 77.741(4)°.
Volume	1488.9(3) $Å^3$
Z	2
Density (calculated)	1.671 Mg/m^3
Absorption coefficient	0.744 mm^{-1}
F(000)	756
Crystal size	0.15 x 0.05 x 0.03 mm^3
Theta range for data collection	1.701 to 25.968°.
Index ranges	-9<=h<=9,-10<=k<=15,-19<=l<=19
Reflections collected	18296
Independent reflections	5655[R(int) = 0.0588]
Completeness to theta =25.968°	97.00%
Absorption correction	Empirical
Max. and min. transmission	0.978 and 0.878
Refinement method	Full-matrix least-squares on F^2
Data / restraints / parameters	5655/ 0/ 400
Goodness-of-fit on F2	1.038
Final R indices [I>2sigma(I)]	R1 = 0.0493, wR2 = 0.1162
R indices (all data)	R1 = 0.0741, wR2 = 0.1293
Largest diff. peak and hole	1.123 and -0.578 e.$Å^{-3}$